matography. The pyrolysis temperature program (300–550°C at 20°C/min followed by 2.5 minutes at 550°C) was controlled by a custom made unit. The GC temperature program was: initial time 27 minutes at 30°C, ramp from 30–300°C at 4.5°C/min, hold at 300°C for 20 minutes.

Data analysis was carried out using HP-chemstation software. Determination of the proportions of gas-range ($C_{1–5}$) and oil-range (C_{6+}) components was carried out by construction of a horizontal baseline on blank-subtracted pyrograms at the zero-level before elution of the C_1 peak, and splitting the integrated chromatogram into a $C_{1–5}$ (gas) and a C_{6+} (oil) fraction (Pepper & Corvi 1995).

Multivariate regression analysis

Multivariate regression analysis was used to evaluate the data obtained from the petrographic and screening analyses (Rock-Eval, LECO) carried out on 54 samples from the coal seams in the Søgne Basin. Data from the previously investigated West Lulu-2 well (Petersen *et al.* 1996) were included ending up with a total of 94 samples. The variables (macerals, maceral groups, microlithotypes, TOC values) used in the multivariate calibration were the normalised data from the maceral group, maceral and microlithotype analyses together with the TOC and T_{max} values. The target parameter to which correlation was performed was the S_2 value. In a study by Petersen *et al.* (1996) the hydrocarbon generative potential represented by S_1+S_2 was used as target parameter. However, as S_1 may vary in a way that is not entirely related to the composition of the organic material, but probably also due to primary migration, it was decided in this study only to correlate to S_2, which is taken to represent the remaining hydrocarbon generative potential. The scope of the correlation is to obtain information on the relation between the remaining generative potential and the composition of the organic matter, and thus to identify the petrographic constituents which are likely to be responsible for petroleum generation in the coal seams.

The correlation was performed with the PC software Sirius (Kvalheim & Karstang 1987) using partial least squares (PLS) regression analyses (Martens & Næs 1991). The latent variables were verified by cross validation proposed by Wold (1978), and the group memberships were calculated using the so-called 'Soft Independent Modeling of Class Analogies' (SIMCA) algorithms (Wold 1976; Kvalheim & Karstang 1992). Prior to modeling the variables were scaled to unit variances in order to avoid dominance from variables high in variance over variables low in variance but yet with significant influence on the target parameter. By doing this all variables are equally weighted with respect to variance prior to the estimation of their importance on the model, however, care must be taken not to model 'noise' from variables with very low values.

The coals of the Bryne Formation in the Søgne Basin

Sedimentological description and interpretation of the coal-bearing intervals

West Lulu-3 well

Below the carbonaceous succession there are fining upward, very fine-grained to fine-grained sandstones with small-scale trough cross-lamination and ripple cross-lamination (Figs 5, 6). Bioturbation may be present in the uppermost part of the interval. The sandstones are interpreted as fluvial channel deposits (Johannessen & Andsbjerg 1993).

The sandstones are overlain by a succession *c.* 8 m thick that is dominated by carbonaceous shales and characterised by thin coal layers or laminae, coaly debris, rootlets with occasionally coalified leaves and twigs, as well as three coal seams, named from below, seams R1, R1a and T2. Rootlets are also abundant in thin silty intercalations and in flaser-bedded heterolithic siltstone, which shows bioturbation. Seam R1 is *c.* 0.56 m thick and it appears as bright and banded coal with pyrite filling vertical cleats. The seam is gradually followed by black, carbonaceous shale. Seam R1a is only *c.* 0.30 m thick. Coal seam T2 is *c.* 0.71 m thick and contains vertical pyrite veinlets.

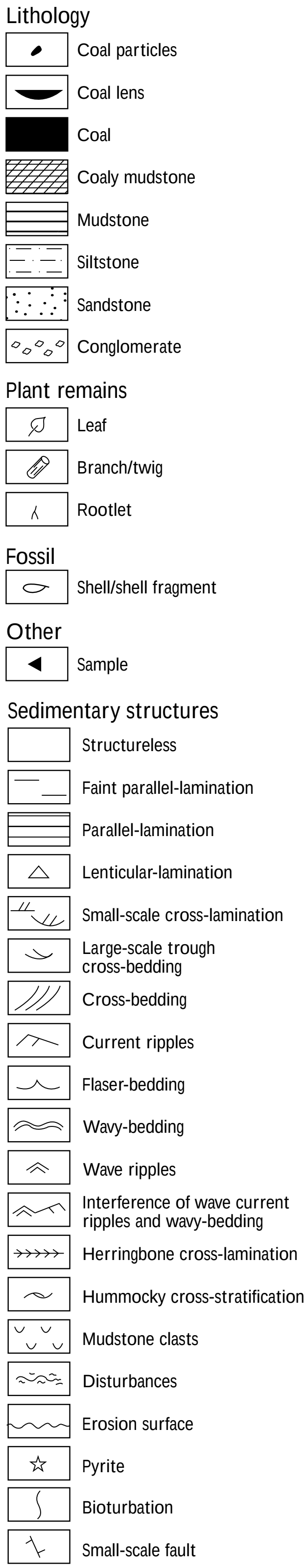

Fig. 5. Explanation of symbols used in the measured well-sections.

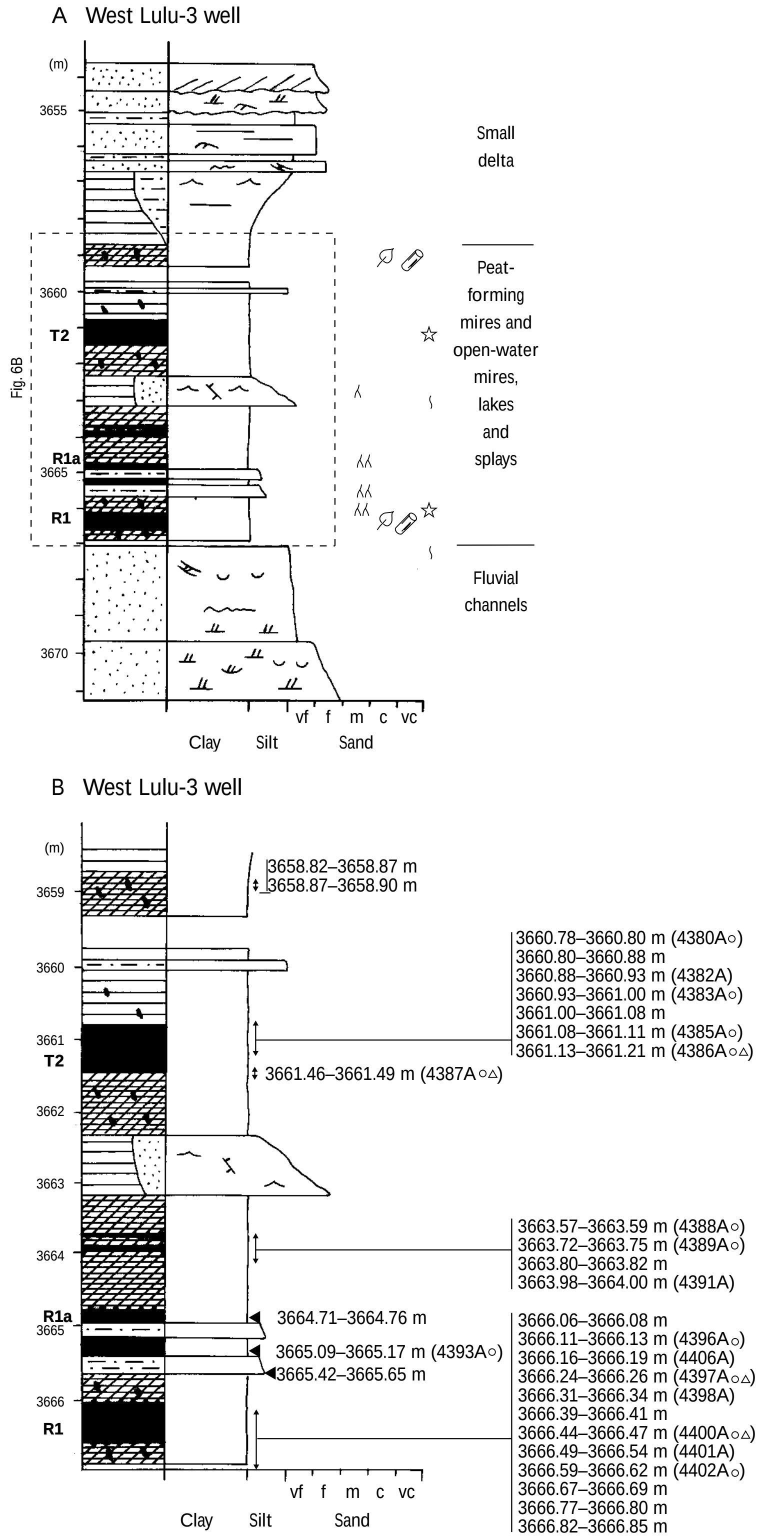

Fig. 6. **A**: The coal-bearing section of the West Lulu-3 well showing the position of seams R1, R1a and T2, and the interpreted depositional environments. **B**: Enlargement of the coal-bearing unit with indication of the sampled intervals. Sample numbers of petrographically analysed samples shown; o: sample analysed by GC and GC/MS; △: sample analysed by Py-GC. For well location, see Fig. 1.

The carbonaceous succession is followed by a coarsening upward succession of heterolithic clay- and siltstone, and sandstone showing mainly faintly parallel-lamination, current ripples and ripple cross-lamination. The sediments were deposited in a lagoon or bay-head delta (Andsbjerg 1997).

West Lulu-1 well

Lowermost in the investigated interval are well-sorted, fine-grained, grey, sandstone beds showing trough cross-bedding, current- and wave-ripple cross-lamination, occasionally hummocky cross-stratification, and bioturbation structures (Fig. 7). The sediments are interpreted to have been deposited in a wave-influenced minor mouth bar.

The sandstone beds are overlain by a complex succession of carbonaceous mudstones and three coal seams, named from below, R1, R1a and T2. Seam R1 is *c.* 0.89 m thick. It starts with mainly bright–dull, banded coal but becomes more bright towards a *c.* 0.11 m thick vitrinite-rich, clayey coal layer in the upper part of the seam (Table 5). Seam R1 ends with bright and dull coal.

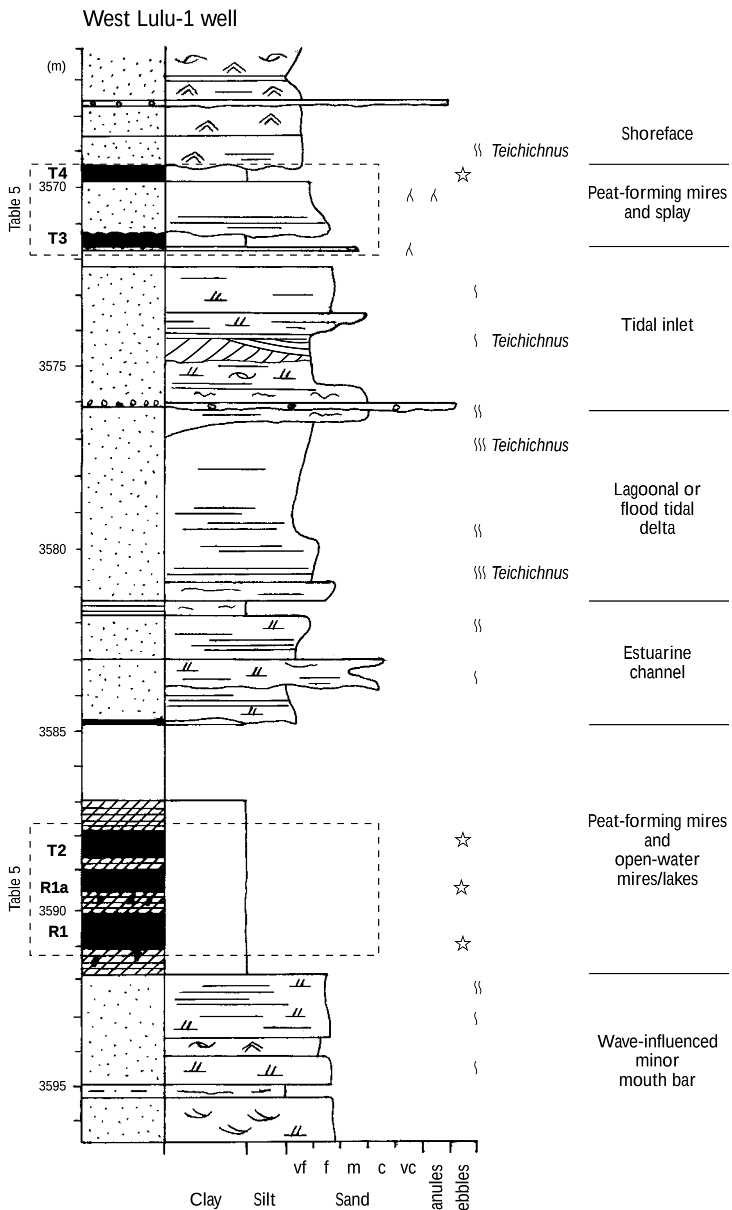

Fig. 7. The coal-bearing section of the West Lulu-1 well showing the position of seams R1, R1a, T2, T3 and T4, and the interpreted depositional environments. See Fig. 5 for legend, Table 5 for detailed description of the sampled intervals, and Fig. 1 for well location.

Small pyrite crystals and horizontal and nearly vertical pyrite veinlets are observed throughout the seam. Clayey coal and black, hard carbonaceous mudstone with vitrinite laminae or lenses and fusinite particles overlie seam R1. The following approximately 0.58 m thick seam R1a shows a trend from bright coal in the lower part to banded coal and clayey coal with vitrinite laminae in the upper part (Table 5). Pyrite has been observed as vertical laminae. Carbonaceous mudstone with vitrinite lenses and an increasing content of clay overlies seam R1a. The *c.* 0.66 m thick seam T2 consists in the basal part of mainly dull coal, where pyrite may be present (Table 5). The middle part is brighter and contains pyrite, while the upper part is composed of hard, dull coal, probably with pyrite.

A 13 m thick succession of poorly sorted, mainly fine-grained sandstone with coarser-grained intervals overlies the organic-rich complex (Fig. 7). The sandstone beds in the lowermost part of the succession have erosional bases and contain ripple cross-lamination and current ripple structures. The sandstones are interpreted to represent estuary channel deposits. Approximately 5 m of mainly upward coarsening, faintly parallel laminated, *Teichichnus* bioturbated sandstone is interpreted to represent lagoonal or flood tidal delta deposits. Uppermost in the sandstone succession is a 4 m thick, erosionally based sandstone unit, that shows a stepwise upward coarsening profile. The unit consists of heterolithic sandstone dominated by hummocky cross-stratification and sandstone showing swaley cross-stratification and low angle cross-bedding. This unit is interpreted as wave-dominated mouth bar and tidal inlet deposits.

The uppermost rooted sandstone is overlain by seam T3, *c.* 0.66 m thick. The lower part of the seam is hard and dull, but it becomes more banded and bright in the upper part (Table 5). An erosional boundary separates it from the overlying sandstone and the *c.* 0.48 m thick seam T4 composed of banded coal, possibly containing pyrite. Seam T4 is erosionally overlain by mainly very fine-grained to fine-grained sandstone beds showing wave ripple, hummocky cross-stratification, current ripple and ripple cross-lamination structures. The sediments were deposited in a shoreface environment.

Lulu-1 well

The investigated interval constitutes part of the Interdistributary Bay Association of Frandsen (1986) and the sediments were mainly interpreted to represent crevasse splays. However, they have more recently been re-interpreted by Johannessen & Andsbjerg (1993) and Andsbjerg (1997).

The siliciclastic sediments underlying the coal seam R1 consist primarily of light to dark grey, mainly structureless, bioturbated silt- and sandstone beds (Fig. 8). The sediments contain small pyrite concretions, organic debris and coalified leaves and twigs. The sediments are interpreted to represent estuary channel and lagoonal deposits (Andsbjerg 1997).

The overlying coaly interval contains grey to black siltstone layers and thin coal layers with rootlets descending into the underlying siltstones. Seam R1 between 3599.43–3599.49 m is composed of banded to dull coal with visible pyrite. A siltstone to very fine-grained sandstone with current ripples and trough cross-bedding is overlying the coaly interval. Rootlets penetrate the sediments from the overlying coal seam T2. The seam is *c.* 0.56 m thick and contains a *c.* 0.08 m thick silt layer approximately in the middle part. The coal below the silt layer is bright in the basal part, and becomes dull towards the top, whereas the coal above the silt layer generally is dull and banded. Immediately above and below the silt layer small pyrite concretions are present in the coal.

Seam T2 is overlain by a siltstone, followed by a thin coal layer, which is erosively overlain by a bioturbated siltstone bed. Above that is a 8 m thick coarsening upward succession. Above a basal mudstone follow well-sorted, very fine- to fine-grained, light to grey and bioturbated sandstones that show wave ripples, trough cross-bedding, current ripples and hummocky cross-stratification. Towards the top the sandstone becomes parallel laminated, and rootlets descend from the overlying seam T4. The sediments represent a prograding shoreface and beach (Johannessen & Andsbjerg 1993). Seam T4 is *c.* 0.36 m thick and consists of banded–bright coal and dull coal with vitrinite laminae. A succession of mainly fine-grained sandstone beds with biotubation and predominately current ripples, hummocky cross-stratification and faintly parallel lamination overlies seam T4.

Amalie-1 well

The coaly interval between 5070.75 m and 5071.72 m overlies a homogeneous mudstone, interpreted to represent a lagoonal environment, which towards the coaly interval is black and carbonaceous with coal lenses and

Table 5. Macroscopic description of samples from West Lulu-1

Seam T4, 0.48 m (3569.39–3569.87 m):	
3569.39–3569.41 m, (4468A oΔ):	Dull-bright banded coal, possibly with pyrite
3569.54–3569.59 m, (4469A oΔ):	As above
3569.66–3569.72 m, (4470A):	Dull-bright banded to dull coal; pyrite possibly present
Seam T3, 0.43 m (3571.32–3571.75 m):	
3571.32–3571.44 m:	Dull-bright banded coal, mainly dull
3571.44–3571.49 m, (4472A o):	Hard and black bright to dull coal
3571.49–3571.57 m, (4473A oΔ):	Mainly bright coal
3571.62–3571.70 m:	Hard, dull coal with vitrinite particles or laminae
3571.70–3571.75 m, (4475A oΔ):	Hard, dull coal
Seam T2, 0.66 m (3587.98–3588.64 m):	
3587.98–3588.08 m, (4476A):	Hard, dull coal with pyrite(?) and vitrinite lenses
3588.08–3588.11 m:	Hard, dull coal
3588.21–3588.28 m, (4478A oΔ):	Dull (to bright) coal, probably with pyrite
3588.28–3588.33 m:	Mainly bright coal with pyrite
3588.33–3588.46 m, (4480A o):	Mainly bright coal
3588.46–3588.54 m, (4481A):	Hard, clayey dull coal or coaly mudstone
3588.54–3588.59 m:	Dull coal with vitrinite particles and lenses
3588.59–3588.64 m, (4483A):	Bright to dull coal with pyrite
(3588.64–3589.05 m, carbonaceous mudstone with vitrinite lenses; not sampled)	
Seam R1a, 0.58 m (3589.05–3589.63 m):	
3589.05–3589.07 m:	Carbonaceous mudstone or clayey coal with vitrinite laminae
3589.07–3589.12 m, (4485A o):	Bright-dull banded coal
3589.12–3589.17 m:	Dull coal with vitrinite laminae; pyrite present
3589.17–3589.22 m, (4487A o):	Mainly bright coal
3589.22–3589.35 m:	Mainly bright coal with duller layers; pyrite present in vertical cleats
3589.35–3589.40 m, (4489A):	Mainly bright coal
3589.40–3589.48 m:	As above
3589.58–3589.63 m, (4491A o):	Bright coal
3589.63–3590.29 m, hard, dark grey-black carbonaceous mudstone and clayey coal with vitrinite lenses and laminae:	
3589.68–3589.71 m:	Hard, black and dull with vitrinite laminae
3589.76–3589.78 m:	Hard and black with vitrinite laminae; fusinite particles observed
3589.96–3589.99 m:	As above
3590.21–3590.29 m, (4495A o):	Carbonaceous mudstone or clayey coal with vitrinite laminae
Seam R1, 0.89 m (3590.29–3591.18 m):	
3590.29–3590.39 m:	Dull and bright coal with clay laminae, fusinite particles present
3590.52–3590.57 m, (4497A):	Dull coal with vitrinite laminae, pyrite present
3590.57–3590.59 m, (4498A o):	Mainly bright coal, small pyrite crystals present
3590.59–3590.65 m, (o):	Carbonaceous mudstone with vitrinite laminae or particles
3590.65–3590.70 m:	Vitrinite-rich carbonaceous mudstone or clayey coal
3590.70–3590.75 m, (4501A o):	Hard, dull coal
3590.75–3590.80 m:	Mainly bright coal; horizontal pyrite lens and small pyrite crystals
3590.80–3590.82 m, (4503A o):	Mainly bright coal
3590.82–3590.87 m, (4504A):	Mainly bright coal with pyrite in almost vertical cleats
3590.87–3590.93 m:	Hard mainly dull coal
3590.93–3590.98 m, (4506A o):	Mainly bright coal
3590.98–3591.08 m, (4507A o):	Bright-dull banded coal; pyrite present
3591.08–3591.13 m:	Bright-dull banded coal
3591.13–3591.18 m, (4509A):	Mainly bright coal with dull laminae
3591.18–3591.92 m, carbonaceous mudstone:	
3591.18–3591.23 m, (o):	Dull carbonaceous mudstone, top more coaly
3591.23–3591.31 m:	Dull carbonaceous mudstone with vitrinite lenses

Samples analysed petrographically are indicated by sample number in brackets. o: sample extracted, fractionated and analysed by means of GC and GC/MS; Δ: sample analysed by means of Py-GC.

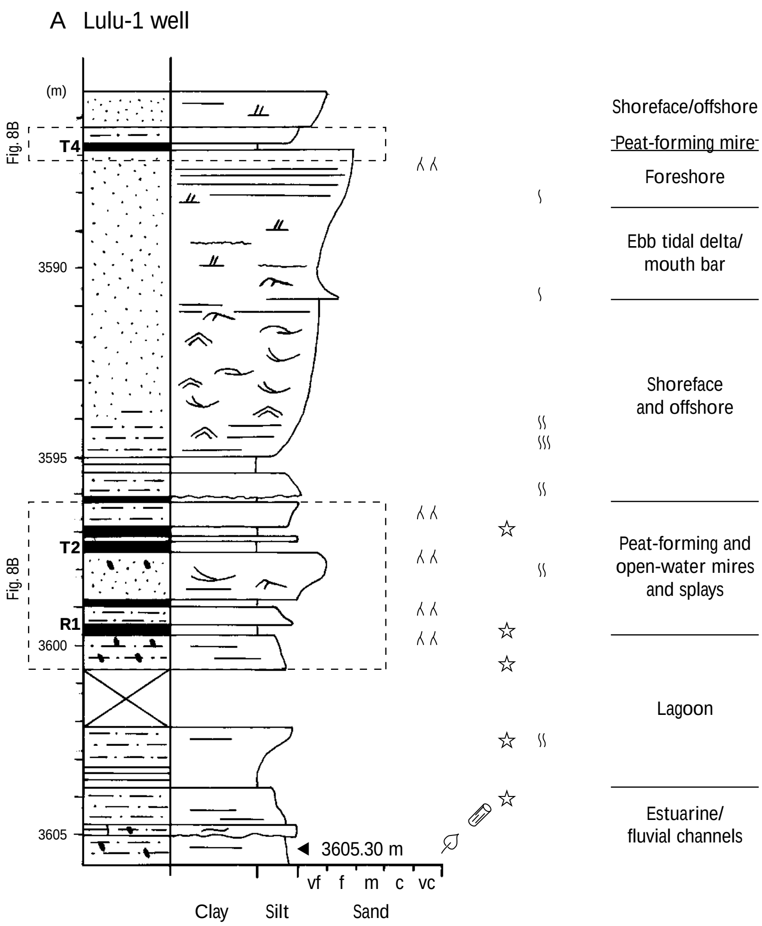

Fig. 8. **A**: The coal-bearing section of the Lulu-1 well showing the position of seams R1, T2, and T4, and the interpreted depositional environments.
B: Enlargement of the coal-bearing units with indication of the sampled intervals. Sample numbers of petrographically analysed samples shown; o: sample analysed by GC and GC/MS; △: sample analysed by Py-GC.
See Fig. 5 for legend and Fig. 1 for well location.

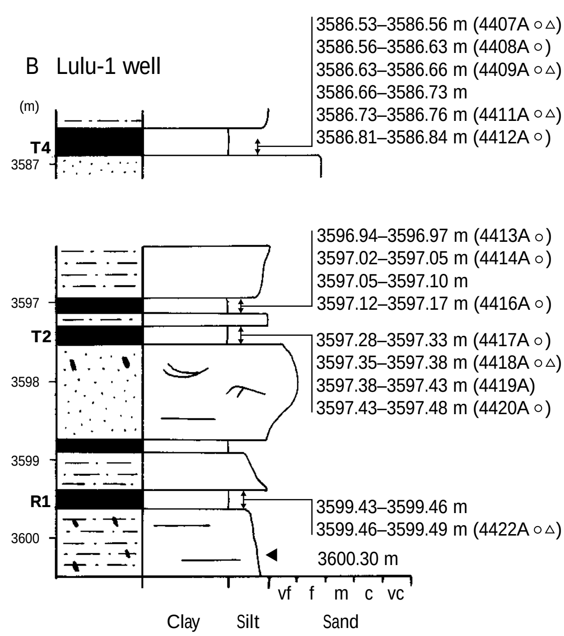

laminae (Fig. 9). The coaly interval consists of only an 0.08 m thick coal layer composed of dull coal with vitrinite laminae. The seam is overlain by a 0.22 m thick coaly mudstone layer, and finally the 0.25 m thick coal seam R1 of mainly dull coal with vitrinite laminae. A 23 m thick succession separates seam R1 from seam T4. Immediately above seam R1 is a 0.5 m thick bed of heterolithic clay- and siltstone interpreted as deposited in a lagoon. Above that the lower part of the succession consists of two erosionally based, fining upward sandstone units that show cross-bedding, ripple cross-lamination, bidirectional ripple cross-lamination, flaser-bedding and wavy-bedding. Rip-up mudstone clasts are present above basal erosion surfaces. On top of the lowermost fining upward unit (5067.7 m) is a structureless mudstone and a 0.15 m thick coaly mudstone, and on top of the second unit (5063.5 m) a 0.4 m thick coaly mudstone. The fining upward sandstone units are interpreted as tidal creek or tidally-influenced fluvial channel deposits, possibly with interbedded tidal

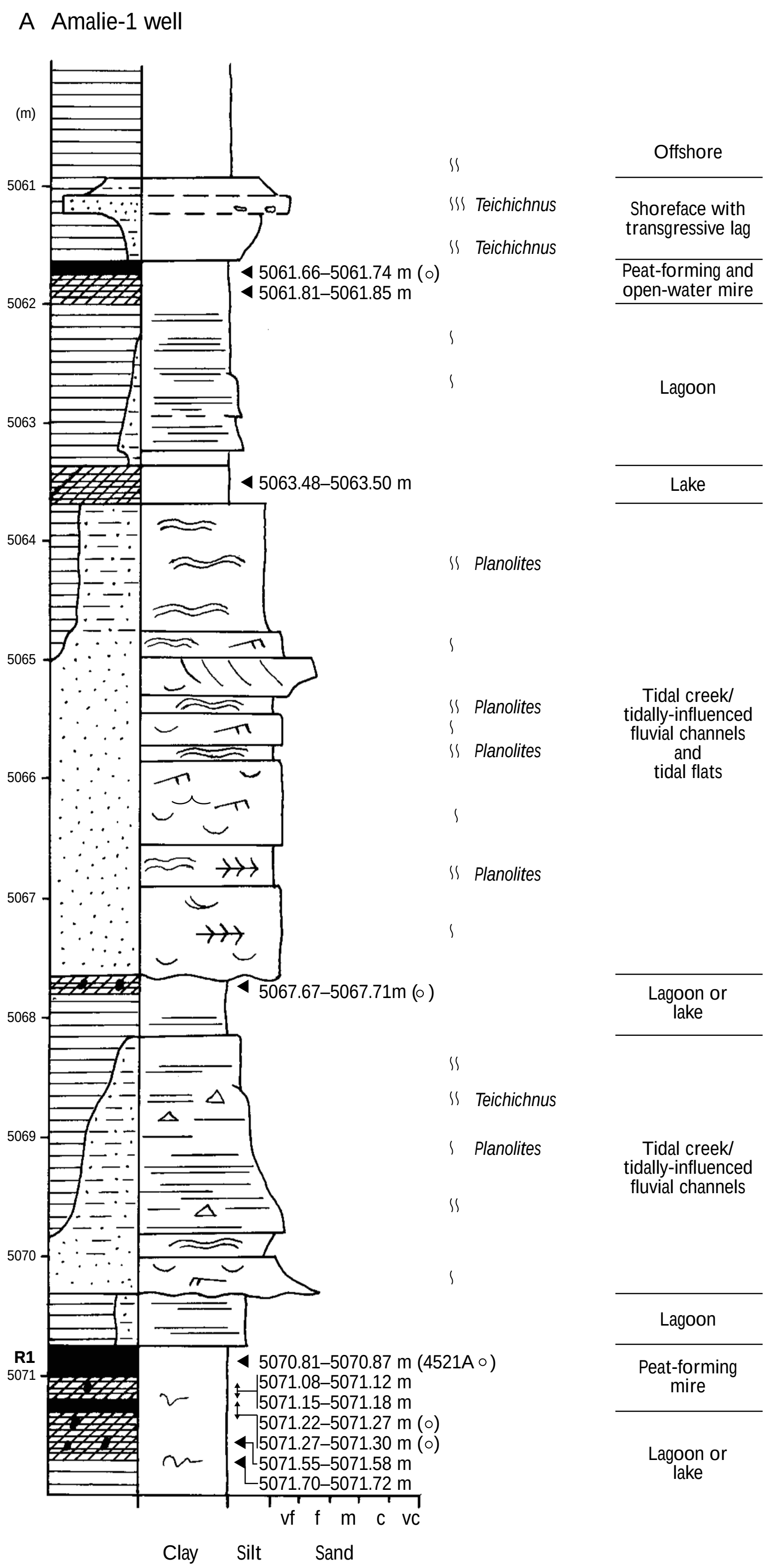

Fig. 9. **A** and **B**: The coal-bearing sections of the Amalie-1 well showing the position of seams R1 and T4, and the interpreted depositional environments. Sample numbers of petrographically analysed samples shown; o: sample analysed by GC and GC/MS; △: sample analysed by Py-GC. See Fig. 5 for legend and Fig. 1 for well location.

Fig. 9. cont.

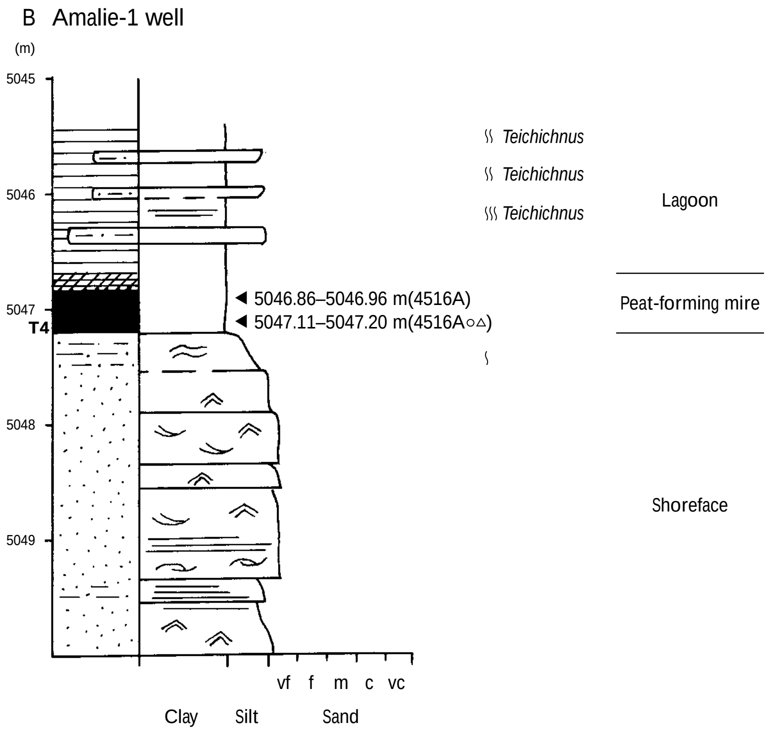

flat sediments in the upper unit (Andsbjerg 1997). *Teichichnus* and *Planolites* burrows have been recognised in the channel deposits. Above the fining upward units is a 2.5 m thick succession of heterolithic siltstone and mudstone, which at the top coarsens upward to a 0.3 m thick sandstone bed. A carbonaceous mudstone with a 0.08 m thick layer of bright coal is present at the base of the coarsening upward unit. This succession is interpreted to be interbedded lagoon and wash-over deposits. The uppermost sandstone bed may represent a transgressive shelf deposit. This succession (Fig. 9A) is separated from the succession shown in Figure 9B by an approximately 10 m thick generally coarsening upward mudstone to sandstone succession interpreted as shoreface deposits. A 2.5 m thick erosionally based unit of very fine- and fine-grained sandstone dominated by wave ripple cross-lamination, hummocky cross-stratification, swaley cross-stratification and possibly low-angle cross-bedding underlies seam T4 (Fig. 9B). This uppermost coarsening upward part of the shoreface succession is interpreted to be progradational shelf and shoreface deposits (Andsbjerg 1997).

The *c.* 0.35 m thick coal seam T4 composed of hard and bright coal overlies the shoreface sandstones. The seam is overlain by highly *Teichichnus* bioturbated clay- and siltstone deposited in a lagoonal environment.

Cleo-1 well

The lowermost part of the succession consists of a siltstone to very fine-grained sandstone. However the crushed core interval hinders recognition of sedimentary structures (Fig. 10). It is overlain by a generally homogeneous, light grey, grey and dark grey mudstone, with common coal particles. Occasional sediment disruption may be related to bioturbation. Rootlets occur in a narrow horizon characterised by coal streaks. The mudstone is overlain by a faintly parallel-laminated, but generally very disturbed, silt- to very fine-grained sandstone with abundant coal particles, streaks and lenses, and coalified wood. Rootlets are also present. The succession is topped by a more sandy, but also very coaly interval. The mudstones with evidence of vegetation are interpreted to represent distal floodplain to shallow lake or pond deposits, while the overlying sandstones were deposited in fluvial, possibly tidally influenced, channels.

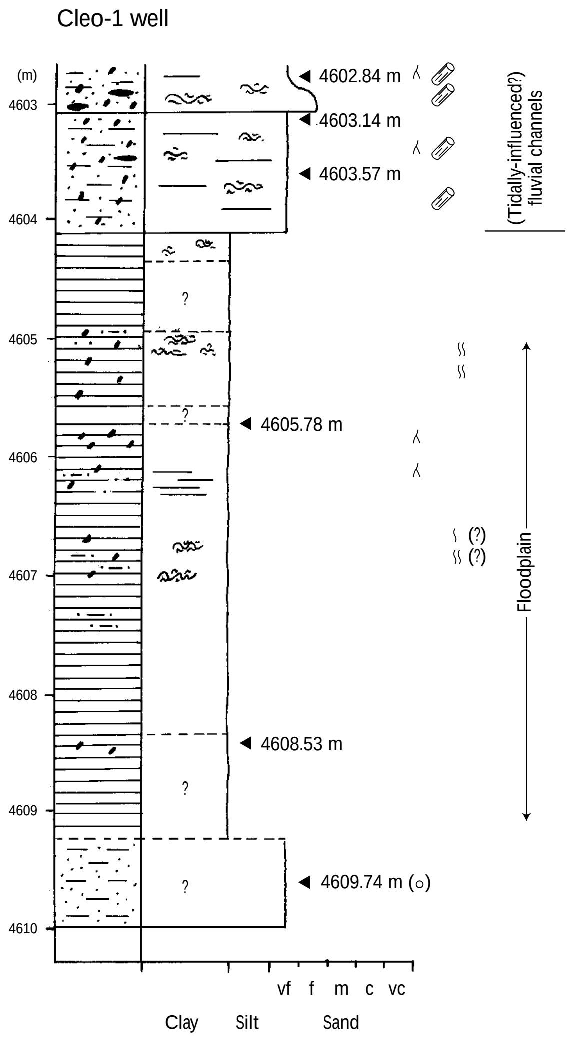

Fig. 10. Sedimentological log of the measured part of the Cleo-1 well showing the interpreted depositional environments. Collected samples shown; o: sample analysed by GC and GC/MS. See Fig. 5 for legend and Fig. 1 for well location.

Sequence stratigraphic framework and spatial coal seam distribution

A sequence stratigraphic interpretation of the coal-bearing interval in the West Lulu-2 well and correlation of the coal-bearing strata between wells within the Søgne Basin has been presented by Petersen & Andsbjerg (1996) and Petersen *et al.* (1996). These studies focused on a detailed organic petrographic and geochemical investigation of the six coal seams and their relationship to sequence stratigraphic key surfaces and systems tracts. This sequence stratigraphic framework was revised somewhat in the more detailed sequence stratigraphic and sedimentological study by Andsbjerg (1997). In the studies by Petersen & Andsbjerg (1996) and Petersen *et al.* (1996) two sequences, A and B, were recognised in the coal-bearing unit of the West Lulu-2 well, with only seam T1 situated in sequence A and the remainding five coal seams situated in the transgressive systems tract (TST) of sequence B (Fig. 11). Seam R1 was situated at the base of the TST and separates the lowstand systems tract (LST) from the TST, and it was thus correlatable to the transgressive surface (TS1). Seam T2 was situated closely above R1 at the very basal part of the TST, whereas seams R2, T3 and T4 were situated close to or include the correlative level to the maximum flooding surface (MFS). In the revised sequence stratigraphic model of Andsbjerg (1997) sequence Bat-1A is equivalent to sequence A of Petersen & Andsbjerg (1996), whereas sequence B of Petersen & Andsbjerg (1996) is subdivided into two sequences, Cal-1A and Cal-1B. The regional sequence boundary (SB) Cal-1A subdivides the Middle Jurassic succession into a lower part dominated by fluvial deposits and an upper part dominated by paralic and shallow marine deposits (Andsbjerg 1997). Only the T1 seam, identified in the West Lulu-2 well, is located below the Cal-1A SB in sequence Bat-1A. The Middle Jurassic sediments above the Cal-1A SB represent sequences Cal-1A, Cal-1B and Cal-1C. The Cal-1B SB separates seams R1 and T2 from seams R2, T3 and T4. However, the five seams R1 to T4 are all located in transgressive systems tracts of their respective sequences. Therefore, coal seams R1–R2 and T2–T4 treated herein are located in sequences Cal-1A and Cal-1B.

In most wells the Cal-1A SB is located at the base of stacked massive channel sandstones. The missing section below the unconformity may amount to up to *c.* 40 m, and the unconformity is interpreted as bounding an incised valley with a relief amounting to at least 40 m. The stacked fluvial and estuarine channel sandstones and interbedded tidal channel and low-energy estuary deposits that constitute the incised valley fill represent the LST and lower TST of the Cal-1A sequence. The valley fill succession is capped by the R1 coal seam, which is also found overlying an interfluvial bypass surface or a very thin (0.5 m) valley-fill unit in the West Lulu-4 well. The upper part of the Cal-1A TST is present above seams R1 and T2 as a thin transgressive shoreface sandstone in the easternmost wells and as a succession of mainly estuarine deposits in the wells to the west. A coarsening upward succession of shelf and

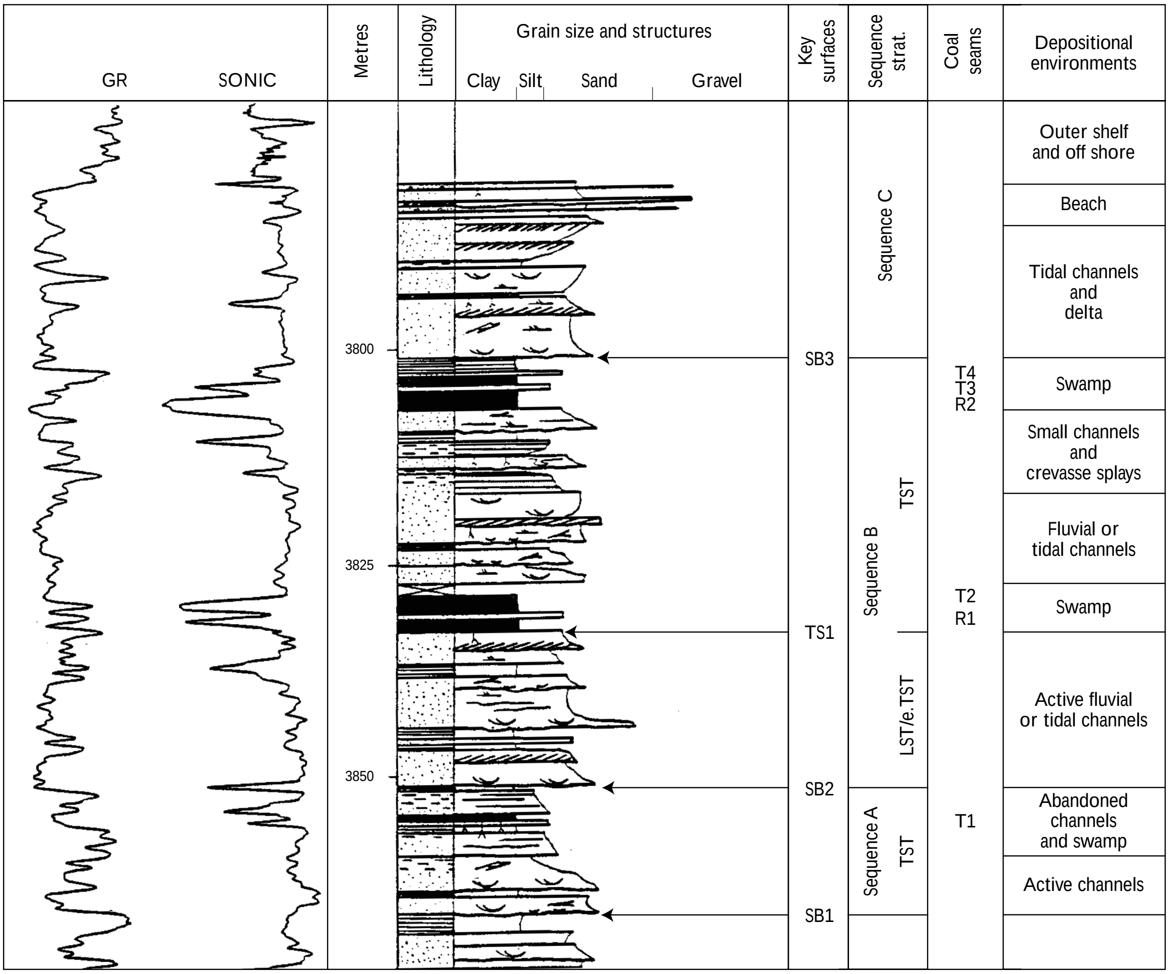

Fig. 11. The coal-bearing section of the West Lulu-2 well showing the position of seams T1, R1, T2, R2, T3 and T4, and the interpreted depositional environments. The coal-bearing unit is bounded by two sequence boundaries (SB1 and SB3) and consists of sequence A, which contains a transgressive systems tract (TST), and sequence B, which contains a lowstand systems tract/early TST and a TST. A transgressive surface (TS) is situated below seam R1. After Petersen *et al.* (1996).

shoreface deposits represents the highstand systems tract (HST) and forced regression systems tract (FRST) of Cal-1A in the easternmost wells (Andsbjerg 1997). In wells in an intermediate position there is a somewhat thinner succession of bay-head or tidal delta deposits, whereas the HST/FRST is missing from the westernmost wells due to erosion at the Cal-1B SB. The Cal-1B SB is located in beach deposits overlying the coarsening upward shoreface succession in the easternmost wells and at the base of tidally influenced channel sandstones in the wells to the west. The beach deposits and lowermost channel sandstones may represent the LST or lowermost TST of Cal-1B. Seams R2, T3 and T4 in the wells to the west and seam T4 seam in the wells to the east are situated on top of these LST/lowermost TST deposits and are thus incorporated in the TST of the Cal-1B sequence.

The sequence stratigraphic framework together with the exellent lateral control provided by the characteristic gamma ray signals of the coal seams helped correlation of the coal intervals. A more detailed coal seam-to-coal seam correlation in the Søgne Basin is possible due to the organic petrographic and geochemical data obtained in the present study (see p. 29). The cored succession in the Cleo-1 well is not included in this correlation; coal seams are absent and the succession prob-

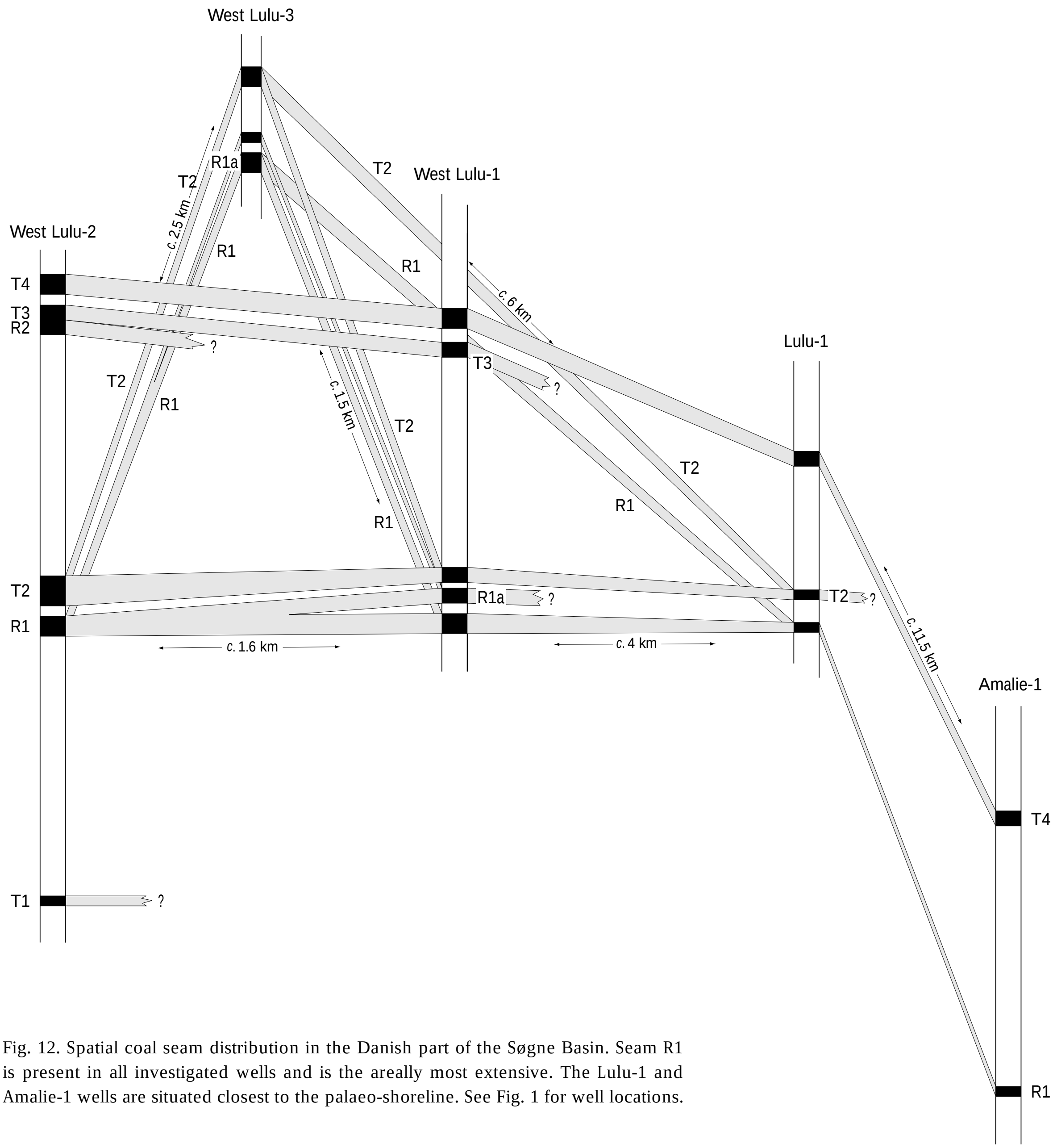

Fig. 12. Spatial coal seam distribution in the Danish part of the Søgne Basin. Seam R1 is present in all investigated wells and is the areally most extensive. The Lulu-1 and Amalie-1 wells are situated closest to the palaeo-shoreline. See Fig. 1 for well locations.

ably belongs to the LST of sequence Cal-1A (Andsbjerg 1997).

The spatial distribution of the coal seams is shown in the fence diagram in Figure 12. Seam T1 in sequence Bat-1A has been observed in West Lulu-2, West Lulu-4 and possibly in Lulu-1. A coal seam is not present at that level in West Lulu-1 and the Norwegian 3/7-4 well and the Bat-1A sequence has been erosionally removed in West Lulu-3. In contrast seam R1 is areally extensive and is present in all wells, which is in accordance with correlation of the seam with a transgressive surface (Fig. 13). In a landward position relative to the palaeo-coastline (West Lulu-2 and West Lulu-1 wells) seam R1 is between *c.* 0.85 and 0.89 m thick (Table 6). In West Lulu-3 the seam is *c.* 0.56 m thick, but basinwards it thins to about *c.* 0.06 m and *c.* 0.25 m in the Lulu-1 and Amalie-1 wells respectively. At 0.66 m above seam R1 in both the West Lulu-3 and West Lulu-1 wells a coal

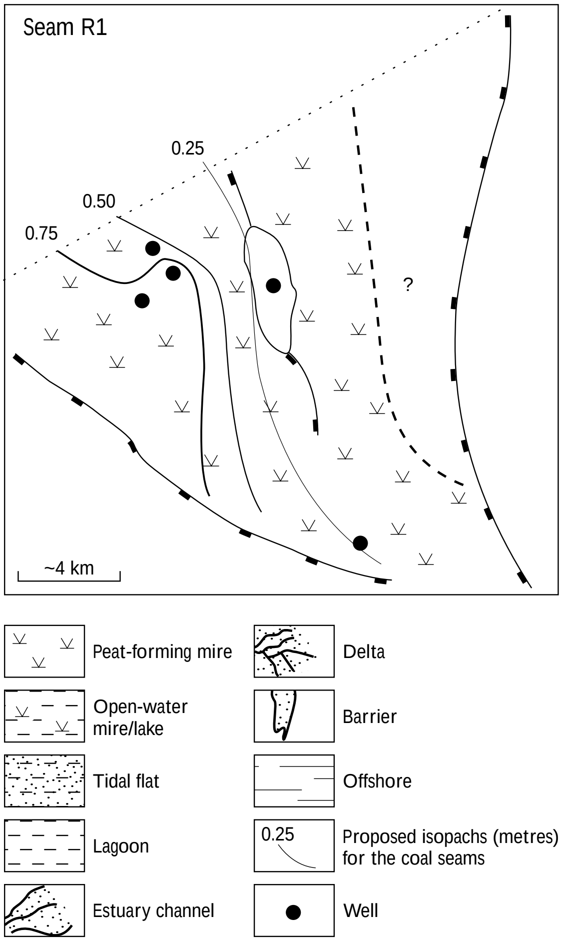

Fig. 13. Palaeogeographic map showing the areal extent of the precursor mire of seam R1 in the Danish part of the Søgne Basin. Isopach-lines show the thickness of coal seam R1 and suggest that the precursor peat deposit thinned towards the palaeo-shoreline and that it had a rather uniform thickness parallel to the ancient coastline. For names and location of the wells, see Fig. 1.

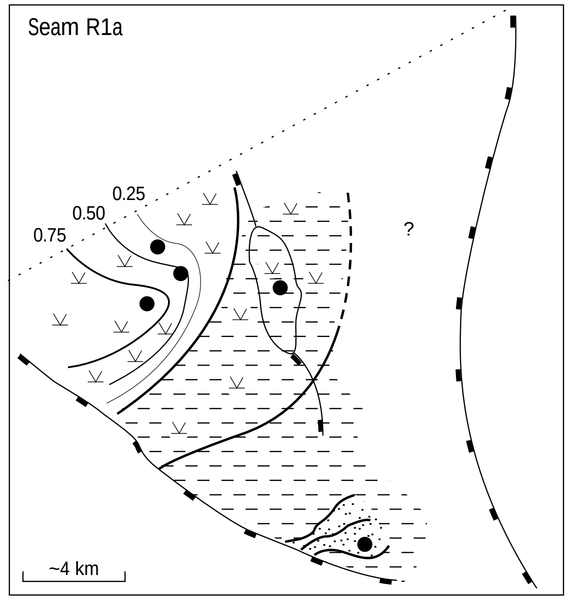

Fig. 14. Palaeogeographic map showing the limited areal extent of the precursor mire of seam R1a. The mire was probably separated from a lagoonal environment towards the south-south-east by an open-water mire or lacustrine environment. For legend, see Fig. 13.

Table 6. Thickness of Bryne Formation coal seams

Well	W. Lulu-2	W. Lulu-3	W. Lulu-1	Lulu-1	Amalie-1
Seam	(m)				
T4	0.50	(0.35?)*	0.48	0.36	0.35
T3	0.94	-	0.66	-	-
R2	1.06	-	-	-	-
T2	1.30	0.71	0.66	0.56	-
R1a	(R1, 0.85)	0.30	0.58	-	-
R1	0.85	0.56	0.89	0.06	0.25
T1	0.40	-	-	-	-
Total	5.05	1.57	3.27	0.98	0.60

*estimated from sonic log

seam named R1a occurs. It is 0.30 m thick in West Lulu-3 and 0.58 m in West Lulu-1. Its organic petrographic and geochemical composition (see below) is intermediate between seam R1 and the overlying seam T2, and it is interpreted to be a split of seam R1. The areal extent of the original peat mire which formed seam R1a was limited (Fig. 14).

Seam T2, situated close to TS1 in the basal part of the TST of sequence Cal-1A, is also laterally extensive. The seam is *c.* 1.30 m thick in West Lulu-2 and thins to *c.* 0.71 m in West Lulu-3 and in a basinwards direction to *c.* 0.66 m in West Lulu-1 and 0.56 m, including a *c.* 0.08 m thick silt layer, in Lulu-1 (Table 6). In contrast to the immediately underlying seam R1, seam T2 is no longer recognisable as coal in the Amalie-1 well, and is probably developed as carbonaceous mudstone. This corroborates the interpretation that the precursor peat of seam R1 formed during relatively slow watertable (base-level) rise related to initial relative sea-level rise allowing peat accumulation to occur over a large area, whereas the T2 peat accumulated during accelerated watertable rise which hindered peat formation at the position of Amalie-1 (Fig. 15; Petersen & Andsbjerg 1996).

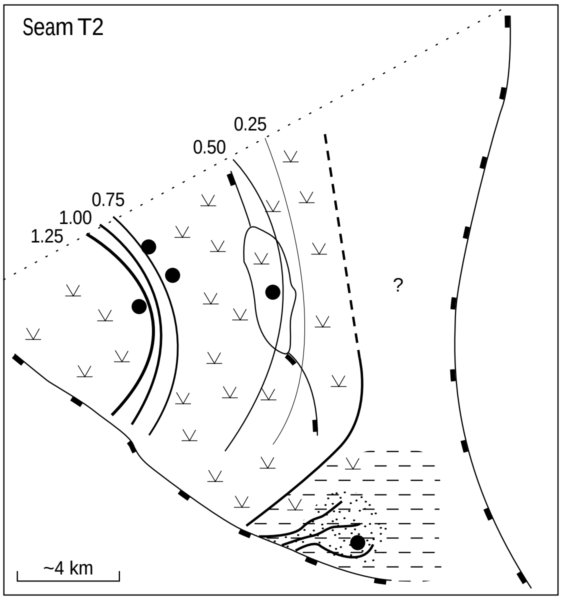

Fig. 15. Palaeogeographic map showing the areal extent of the precursor mire of seam T2. The coal seam thickens towards the north-east where it attains a thickness of 1.3 m. For legend, see Fig. 13.

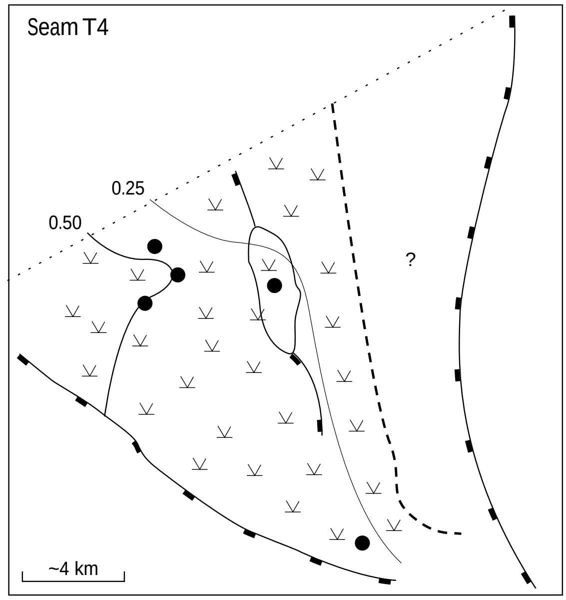

Fig. 17. Palaeogeographic map showing the areally extensive precursor mire of seam T4. Coal isopach-lines suggest that the thichness of the original peat deposit was relatively uniform. For legend, see Fig. 13.

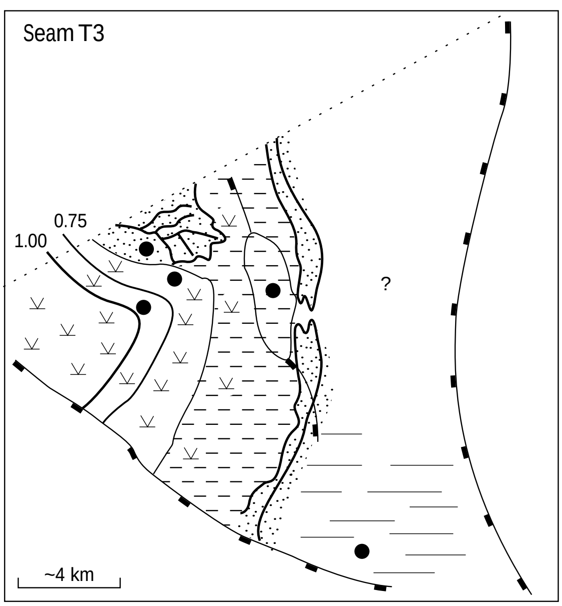

Fig. 16. Palaeogeographic map showing the areal extent of the precursor mire of seam T3. The areally restricted precursor mire of seam T3 was probably protected from the offshore marine environment to the east by barrier islands behind which lagoonal and open-water mire environments prevailed. For legend, see Fig. 13.

In West Lulu-2 a thick coal bed was interpreted to be a composite of two seams, R2 and T3 (Fig. 11; Petersen & Andsbjerg 1996; Petersen *et al.* 1996). This division is no longer recognisable in West Lulu-1 where only seam T3, 0.66 m thick, seems to be present. The areal extent of seam T3 is limited, and during deposition lagoonal, barrier and offshore environments prevailed east of the T3 mire (Fig. 16).

The overlying seam T4 can be followed laterally from West Lulu-2 to Amalie-1. In the most landward position (West Lulu-2) relative to the palaeo-shoreline the seam is *c.* 0.50 m thick, but it thins to *c.* 0.35 m in both Lulu-1 and Amalie-1 (Table 6). Based on the sonic log motif of West Lulu-3, the seam may also be present in that well (Fig. 17).

This suggested spatial coal seam distribution in the Bryne Formation is restricted by the limited number of drilled and cored wells in the Danish part of the Søgne Basin, but wells in the Norwegian part of the Søgne Basin indicate a much larger areal extent of the coal seams. The fence diagram gives an idea of the distribution of the cumulative coal seam thickness in the Søgne Basin. The thickest cumulative seam thickness, 5.05 m, occurs in the West Lulu-2 well positioned most landward relative to the ancient sea, and the total coal seam thickness diminishes in a seaward direction (Fig. 12; Table 6). The part of the ancient peat mires situated closest to the palaeo-shoreline should be favourable for the formation of petroleum-prone organic components due to a continuously high watertable and anoxic conditions (Petersen *et al.* 1996). However, this may be compensated for by the greater total amount of organic matter in the more landward parts of the palaeomires.

Organic petrographic and geochemical results

Vitrinite reflectances

The 16 vitrinite reflectance measurements from the coals in the West Lulu-1, West Lulu-3 and Lulu-1 wells fall in the range 0.75–0.89 %R_m with the lowest reflectance value measured in seam T4 in West Lulu-1 and the highest value measured in Lulu-1 (Tables 7–9). Twelve vitrinite reflectance values of the West Lulu-2 well coals are within the same range, 0.78–0.89 %R_m (Petersen *et al.* 1996). The majority (22) of the 28 reflectance values, however, lie between 0.81 %R_m and 0.89 %R_m. These reflectance values indicate that the coals within the four wells are of high volatile bituminous B/A rank. The 2 vitrinite reflectance values from the Amalie-1 well are significantly higher, both 1.3 %R_m, indicating a medium volatile bituminous rank (Table 10). Vitrinite reflectance measurements on vitrinitic material in Cleo-1 give values of 0.90 %R_m and 0.95 %R_m inferring a high volatile bituminous A rank.

Organic petrographic composition

In the following the organic petrographic composition and lateral development of the seams is presented. With respect to seams T1 and R2, which only occur in the West Lulu-2 well, the reader in referred to Petersen & Andsbjerg (1996) and Petersen *et al.* (1996).

Seam R1. In West Lulu-3 the seam is composed of comparatively high contents of vitrinite and varying amounts of inertinite, vitrite+clarite and the inertinite-rich microlithotypes vitrinertite+durite+clarodurite (Figs 18, 19). Detrovitrinite, including fluorescent collodetrinite, dominates over telovitrinite.

Pyrolytic carbon occurs throughout the seam (see Petersen 1998), and in the interval 28–31 cm oxidised cutinite and unsorted inertodetrinite and macrinite are present. Liptinite constitutes between 1.0 and 4.4 vol.% of the coal and it is composed of liptodetrinite, sporinite, resinite and cutinite with a liptinite maceral only in a few cases exceeding 1.4 vol.%. Pyrite, mainly occurring as minute crystals, generally constitutes 1.0 vol.% or less.

Seam R1 is dominated by vitrinite in the West Lulu-1 well, but the content of vitrite+clarite decreases upwards through the seam while vitrinertite+durite+clarodurite shows an increasing tendency (Figs 18, 19). Collotelinite is weakly fluorescent, and fine-grained allochthonous inertodetrinite occurs disseminated in vitrinite. The liptinite content ranges between 0.8 and 3.2 vol.% and is mainly composed of liptodetrinite, cutinite and sporinite. Pyrite is only present in very small amounts.

Table 7. West Lulu-3 well: GC data, GC/MS data and vitrinite reflectance values

Seam	Sample number	Pr/Ph	CPI	%R_m	Steranes: 29αααS / 29ααα(S+R)	Steranes: 29αββ(S+R) / 29αββ(S+R)+29ααα(S+R)	Steranes: %αββ C_{27}	Steranes: %αββ C_{28}	Steranes: %αββ C_{29}
T2	4380A	5.56	1.09	-	0.39	0.49	18.8	27.2	54.0
	4383A	5.69	1.11	-	0.46	0.50	20.1	30.5	49.4
	4385A	5.19	1.12	-	0.43	0.51	23.5	26.5	50.0
	4386A	5.42	1.09	-	0.44	0.48	21.0	28.4	50.5
	4387A	5.36	1.09	-	0.40	0.47	12.3	27.0	60.7
R1a	4393A	6.17	1.12	-	0.41	0.48	14.6	25.8	59.5
R1	4396A	5.84	1.11	0.88	0.40	0.47	10.0	24.2	65.7
	4397A	5.69	1.11	0.87	0.42	0.51	10.0	23.9	66.2
	4400A	5.81	1.12	0.87	0.43	0.48	10.1	24.2	65.7
	4401A	-	-	0.88	-	-	-	-	-
	4402A	5.74	1.11	-	0.45	0.48	9.1	23.7	67.2
Mudstones	4388A	7.77	1.10	-	0.25	0.37	16.7	20.6	62.7
	4389A	7.48	1.13	-	0.36	0.44	13.4	27.7	58.9

Table 8. West Lulu-1 well: GC data, GC/MS data and vitrinite reflectance values

Seam	Sample number	Pr/Ph	CPI	%R_m	Steranes 29αααS/29ααα(S+R)	Steranes 29αββ(S+R)/29αββ(S+R)+29ααα(S+R)	%αββ C_{27}	%αββ C_{28}	%αββ C_{29}
T4	4468A	3.46	1.06	0.76	0.49	0.62	31.9	28.7	39.5
	4469A	3.01	1.05	0.75	0.47	0.59	31.2	28.6	40.2
T3	4472A	3.65	1.04	-	0.48	0.60	31.9	29.0	39.1
	4473A	3.35	1.06	0.78	0.46	0.63	31.9	29.3	38.8
	4475A	3.62	1.06	0.77	0.47	0.61	31.2	28.2	40.5
T2	4478A	3.26	1.05	-	0.46	0.57	29.7	28.4	41.9
	4480A	2.95	1.04	-	0.46	0.55	30.8	28.4	40.7
R1a	4485A	3.57	1.05	-	0.48	0.57	29.6	27.8	42.6
	4487A	3.45	1.04	-	0.48	0.57	31.0	27.7	41.3
	4491A	3.25	1.04	0.86	0.43	0.51	24.6	28.7	46.7
R1	4498A	3.94	1.04	-	0.46	0.49	17.3	25.5	57.2
	4499A	3.65	1.04	-	0.44	0.47	17.2	26.1	56.7
	4501A	3.10	1.04	-	0.46	0.51	22.5	26.6	50.9
	4503A	3.72	1.05	-	0.47	0.54	23.9	27.8	48.2
	4504A	-	-	0.86	-	-	-	-	-
	4506A	3.71	1.05	0.87	0.48	0.55	23.0	26.9	50.1
	4507A	3.77	1.06	-	0.47	0.52	23.6	27.9	48.5
Mudstones	4495A	3.50	1.03	-	0.45	0.50	20.7	25.8	53.5
	4510A	3.45	1.04	-	0.45	0.51	22.1	26.4	51.6

Table 9. Lulu-1 well: GC data, GC/MS data and vitrinite reflectance values

Seam	Sample number	Pr/Ph	CPI	%R_m	Steranes 29αααS/29ααα(S+R)	Steranes 29αββ(S+R)/29αββ(S+R)+29ααα(S+R)	%αββ C_{27}	%αββ C_{28}	%αββ C_{29}
T4	4407A	3.19	1.08	0.85	0.48	0.63	34.0	29.2	36.7
	4408A	2.58	1.05	-	0.51	0.64	32.7	28.0	39.3
	4409A	2.47	1.06	-	0.50	0.66	34.7	28.3	37.0
	4411A	2.82	1.06	-	0.50	0.62	36.7	27.4	35.9
	4412A	3.59	1.05	-	0.49	0.62	33.7	29.6	36.7
T2	4413A	2.46	1.07	-	0.50	0.64	33.1	28.6	38.2
	4414A	2.74	1.08	0.89	0.49	0.61	35.1	27.1	37.9
	4416A	3.17	1.07	0.77	0.48	0.62	33.9	28.4	37.8
	4417A	2.90	1.05	-	0.49	0.63	35.4	27.6	37.0
	4418A	2.67	1.07	-	0.48	0.62	33.8	29.8	36.4
	4419A	-	-	0.89	-	-	-	-	-
	4420A	2.84	1.07	-	0.50	0.60	36.5	28.4	35.1
R1	4422A	3.11	1.05	0.89	0.46	0.52	22.0	30.3	47.7

Table 10. Amalie-1 well: GC data, GC/MS data and vitrinite reflectance values

Seam	Sample number	Pr/Ph	CPI	%R_m	Steranes 29αααS/29ααα(S+R)	Steranes 29αββ(S+R)/29αββ(S+R)+29ααα(S+R)	%αββ C_{27}	%αββ C_{28}	%αββ C_{29}
T4	4515A	-	-	1.30	-	-	-	-	-
	4516A	2.56	1.15	1.30	0.41	0.49	34.6	29.6	35.8
R1	4521A	3.57	1.09	-	0.46	0.60	35.8	28.3	35.9
Mudstones	4517A	2.96	1.03	-	0.48	0.56	29.7	32.8	37.5
	4520A	1.26	1.13	-	0.49	0.58	23.9	31.8	44.3
	4524A	2.38	1.08	-	0.46	0.54	35.5	30.7	33.8
	4525A	2.56	1.11	-	0.44	0.55	36.9	30.1	32.9

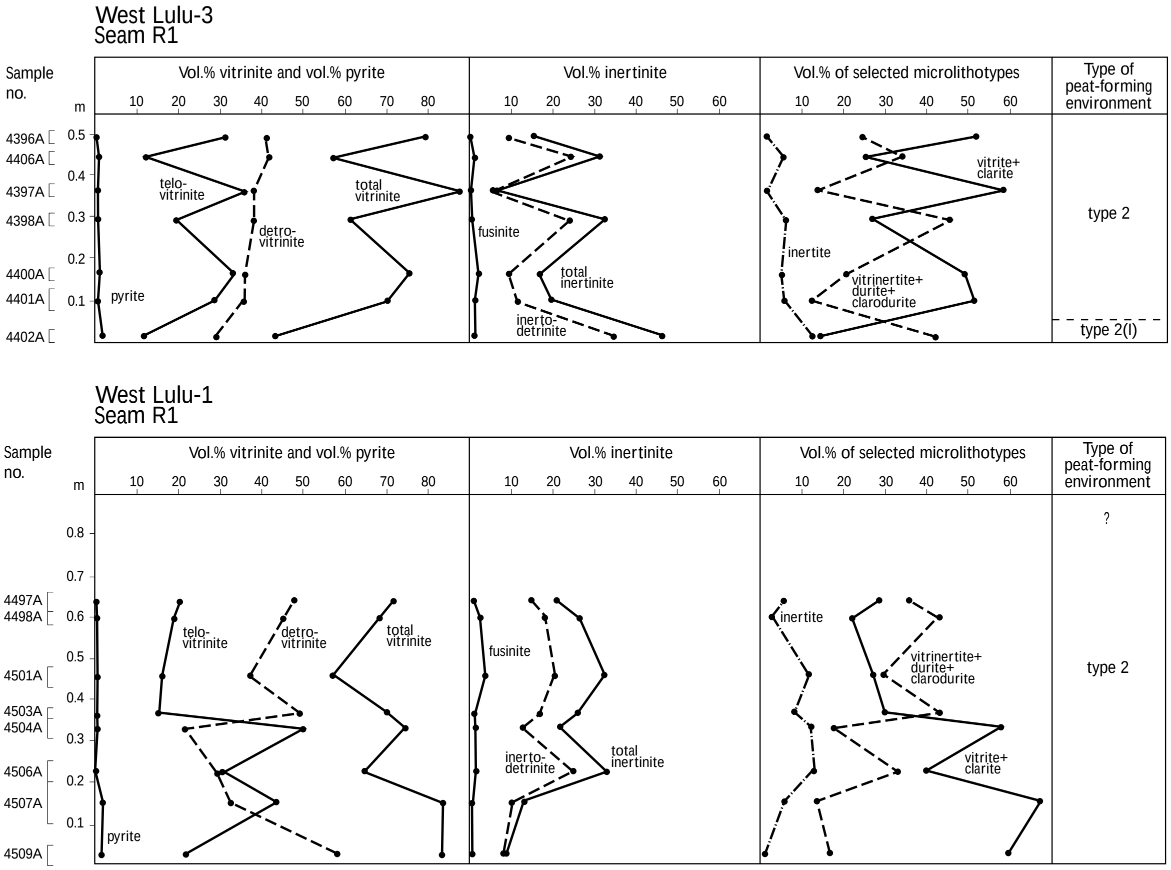

Fig. 18. Coal petrographic composition of seam R1 in the West Lulu-1 and West Lulu-3 wells.

In both Lulu-1 and Amalie-1 seam R1 is dominated by vitrinite (Fig. 19). In Lulu-1 the seam contains significant proportions of vitrite+clarite (65.6 vol.%), and in Amalie-1 vitrinertite (35.8 vol.%), vitrite (28.0 vol.%) and carbominerite (19.4 vol.%). Cutinite, sporinite, liptodetrinite and resinite are recognised in R1 in Lulu-1 whereas the high rank of the coal in Amalie-1 has only allowed the detection of a few liptodetrinites. The pyrite content is in both locations 0.8 vol.%.

Seam R1a. The sample from R1a in West Lulu-3 and the majority of seam R1a in West Lulu-1 is characterised by high contents of vitrinite and the microlithotypes vitrite+clarite (Figs 19, 20). A fusinite peak in the lower and upper part of R1a in West Lulu-1 accounts for coinciding inertite peaks. Char particles have been observed in both levels in the seam, and in R1a in West Lulu-3 pyrolytic carbon is present. The liptinite content ranges between 1.6 and 3.6 vol.% and is composed of liptodetrinite, cutinite, resinite and sporinite. Generally the content of a single liptinite maceral is less than 2.0 vol.%. The pyrite content does not exceed 1.0 vol.%, and except for 10.2 vol.% detrital minerals and 16.6 vol.% carbominerite in R1a in West Lulu-3 the microscopic visible inorganic fraction ranges between 0 and 2.0 vol.%.

Seam T2. In West Lulu-3 seam T2 is characterised by an increase in the contents of inertinite and inertinite-rich microlithotypes followed by a decrease (Figs 19, 21). Total vitrinite content shows also a weak increase but a marked decrease occurs in the level with peak inertinite content. Vitrite+clarite exhibits varying values, however increases in the upper part of T2. The collodetrinite and collotelinite macerals are fluorescent. Char (see Petersen 1998) and oxidised cutinite and resinite are present in several levels in the seam. The liptinite content ranges between 1.6 and 7.8 vol.% and consists of liptodetrinite, cutinite, sporinite, resinite and in the uppermost part of the seam also suberinite. In general the content of individual liptinite macerals does not exceed 1.6 vol.%. The basal part of T2 is rich in detri-

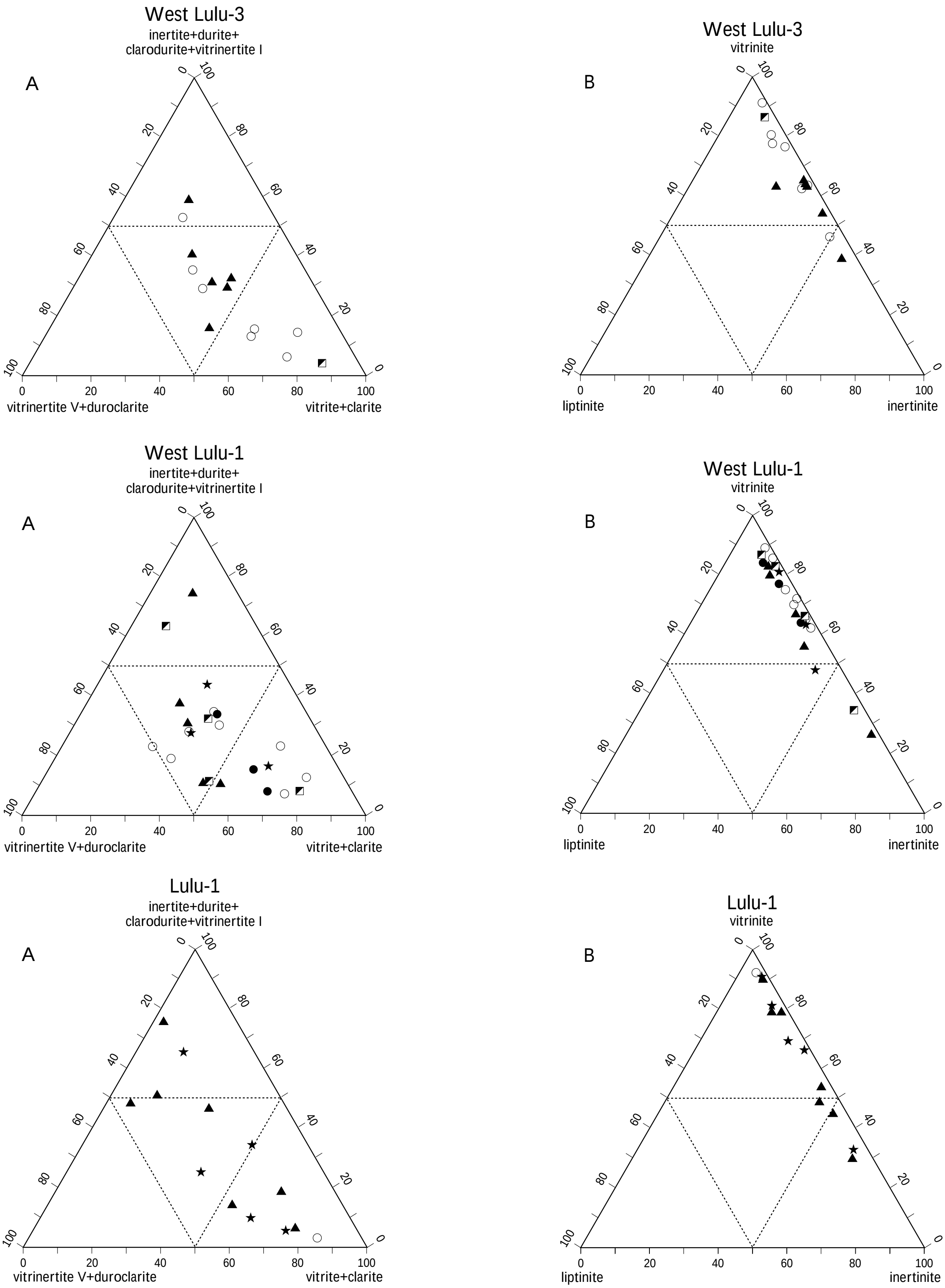

Fig. 19. Triangular plots showing the microlithotype and maceral group composition of seams R1, R1a, T2, T3 and T4 in the West Lulu-3, West Lulu-1, Lulu-1 and Amalie-1 wells.

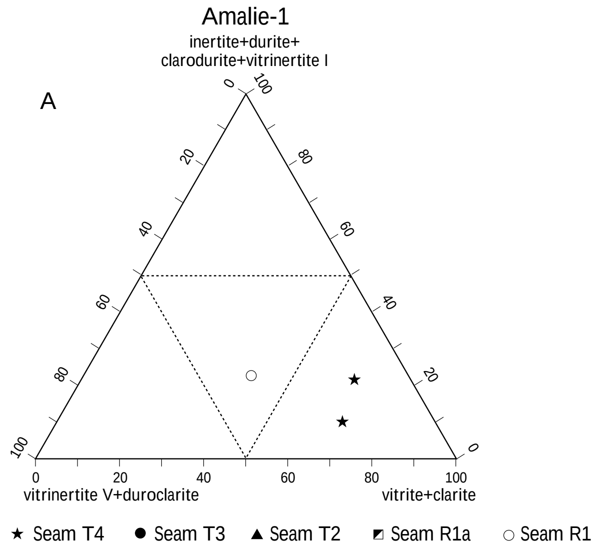

Fig. 19. cont.

tal mineral matter (26.0 vol.%) and carbominerite (41.4 vol.%), while the pyrite content is low or nil.

Seam T2 in West Lulu-1 shows a pronounced decrease in the contents of vitrinite, vitrite+clarite and pyrite up through the seam accompanied by a similar increase in the contents of inertinite and inertinite-rich microlithotypes, in particular inertite (Figs 19, 21). Within the lower part of the seam the inertinite commonly occurs as fine-grained and occasionally micrograded allochthonous inertodetrinite. The liptinite content lies between 2.4 and 6.8 vol.% and consists of liptodetrinite, resinite, sporinite and cutinite. The finely detrital liptodetrinite may occur in association with inertodetrinite. Pyrite varies between 0.2 and 2.0 vol.% and the content of detrital minerals through the seam is, except for one sample, very low (< 1.0 vol.%).

The lower and upper part of seam T2 in Lulu-1 has high proportions of vitrinite and vitrite+clarite while the middle portion is dominated by inertinite and inertinite-rich microlithotypes (Figs 19, 21). The vitrinite fluoresces during blue light irradiation. The inertodetrinite is generally very fine-grained, it may be well-sorted and rounded, and it shows microgradation and microlamination, commonly together with tiny liptodetrinite particles (Figs 22, 23). Groundmass-like macrinite occurs in the interval 33–38 cm, and in the uppermost part char and fusinite occur. Pyrolytic carbon has been observed in the interval *c.* 8–23 cm. Very small fluorescent particles are associated with micrinite-like particles and inertodetrinite. The liptinite content ranges between 1.6 and 5.8 vol.%, with the majority of the samples above 3.0 vol.%. The liptinite fraction consists of lip-

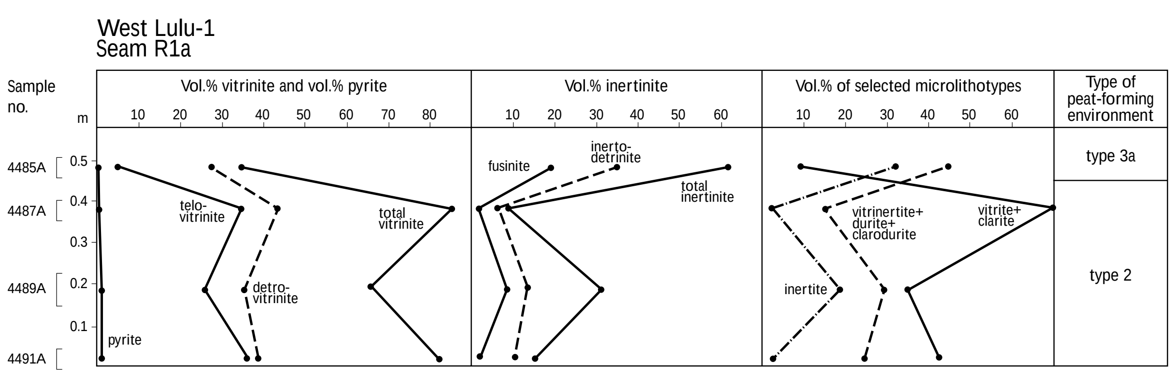

Fig. 20. Coal petrographic composition of seam R1a in the West Lulu-1 well.

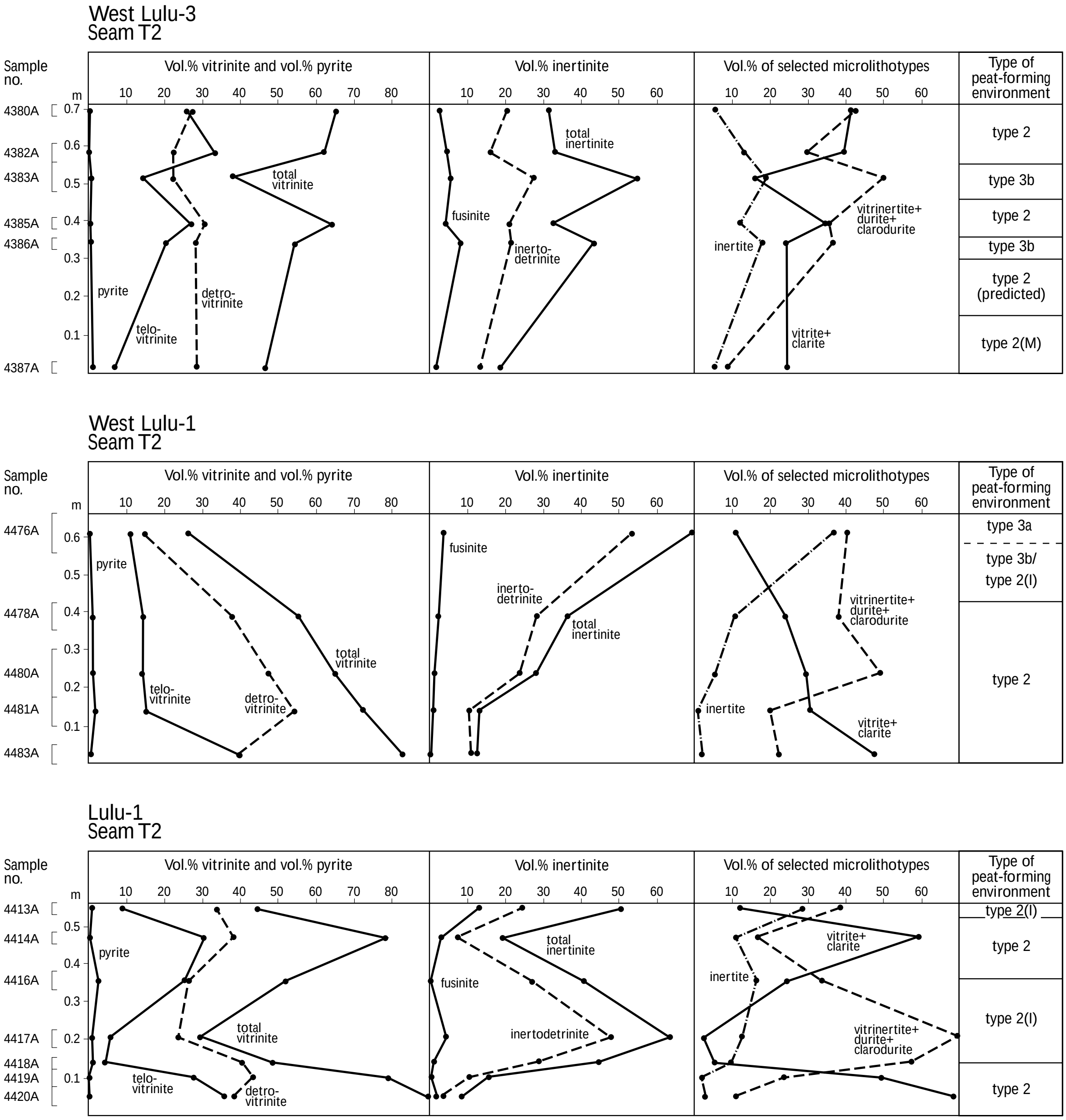

Fig. 21. Coal petrographic composition of seam T2 in the West Lulu-3, West Lulu-1 and Lulu-1 wells.

todetrinite, resinite, sporinite and cutinite. Pyrite, which may be framboidal, ranges between nil and 2.6 vol.%, while detrital minerals constitute less than 1.5 vol.% in all samples.

Seam T3. The seam occurs in West Lulu-1 and is characterised by high contents of vitrinite and vitrite+clarite, although the vitrite+clarite content decreases in the uppermost investigated sample (Figs 19, 24). Inertinite and inertinite-rich microlithotypes show the opposite trend. Char is observed, in particular in the uppermost sample. The vitrinite, generally dominated by telovitrinite (telinite and collotelinite), is strongly fluorescent (Fig. 25), and bitumens are liberated from the vitrinite during blue-light illumination. The liptinite content, varying between 3.4 and 5.0 vol.%, is composed of liptodetrinite, cutinite, sporinite and resinite (Fig. 25). Exsudatinite expelled into a small cleat has been

Fig. 22. Photomicrographs from seam T2 in the Lulu-1 well. **A** and **B**: Examples of microgradeation starting with inertodetrinite and ending with increased amounts of liptodetrinite and vitrinite (sample 4417A, 17.78–22.86 cm). **C**: Micro-cross-lamination; approximate angle of cross-lamination is indicated by puntuated lines (sample 4418A, 12.70– 15.24 cm). All photographs in reflected white light and oil immersion. Scale bar ~ 30 µm.

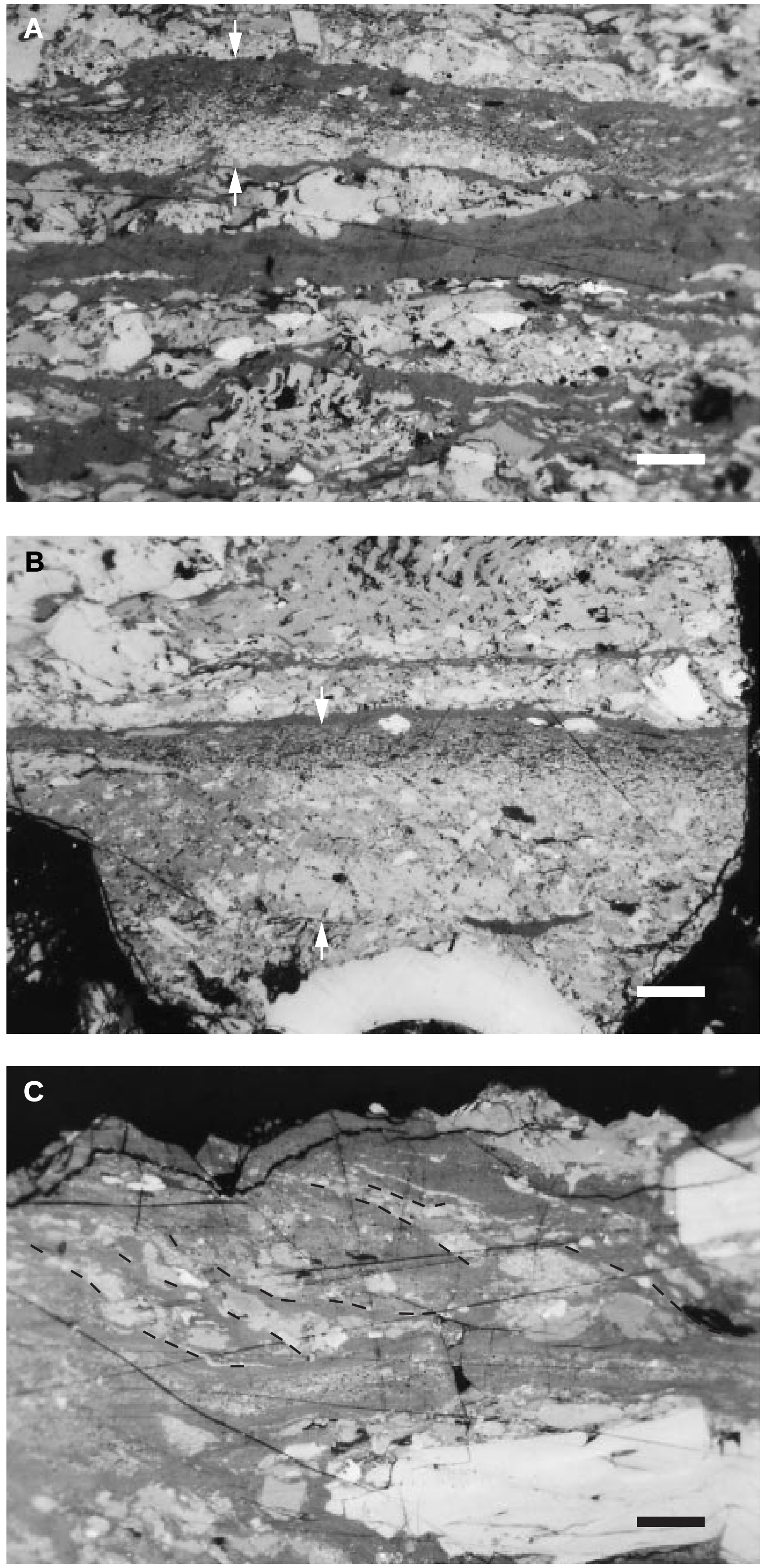

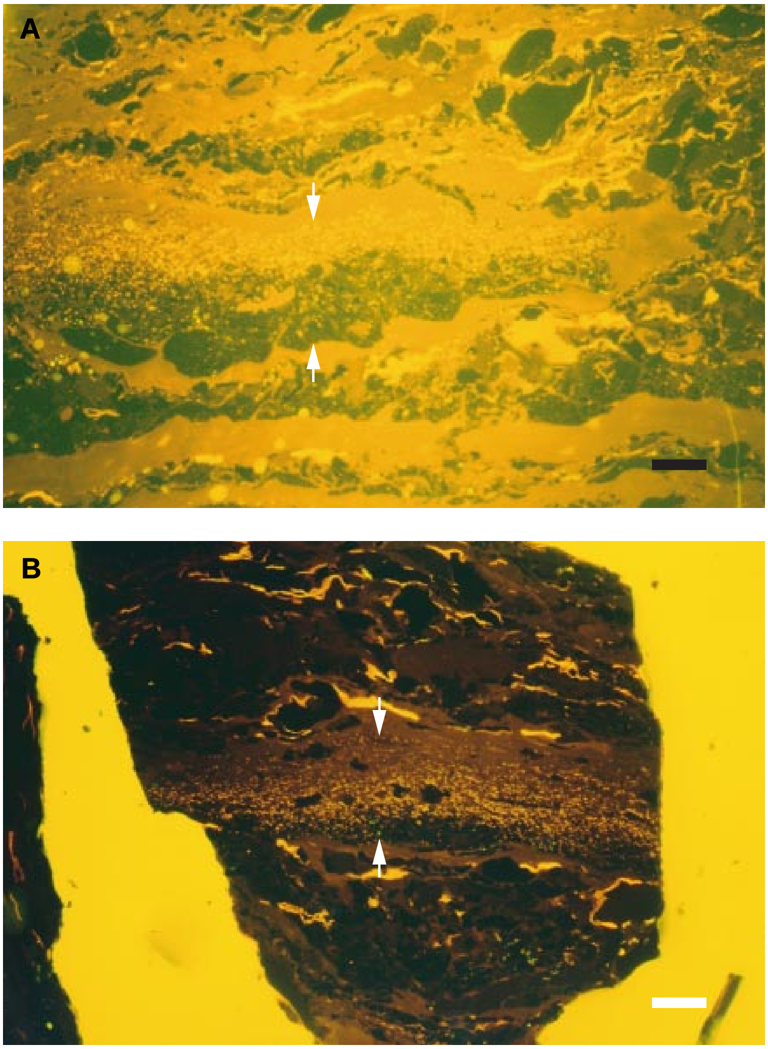

Fig. 23. Photographs from seam T2 in the Lulu-1 well. **A** and **B**: Microgradation shown between arrows; increased proportion of liptodetrinite towards the top of the micrograded lamina is evident from the abundance of tiny yellowish-fluorescent particles (sample 4417A, 17.28–22.86 cm). Note also the fluorescence of the vitrinite bands. Photographs in reflected light, blue-light irradiation and water immersion. Scale bar ~ 30 µm.

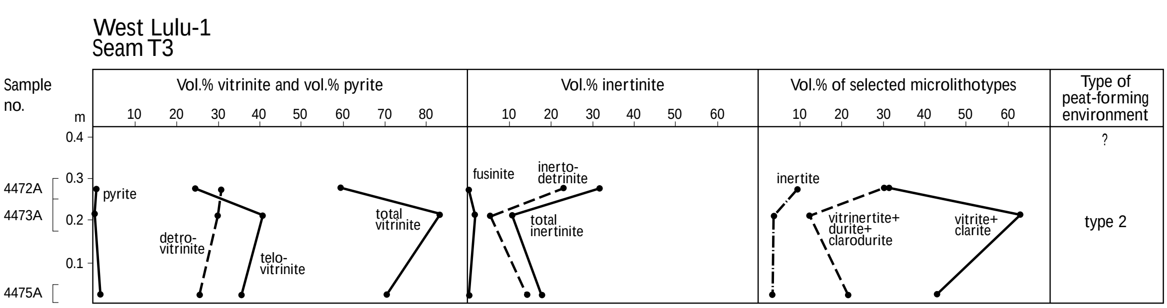

Fig. 24. Coal petrographic composition of seam T3 in the West Lulu-1 well.

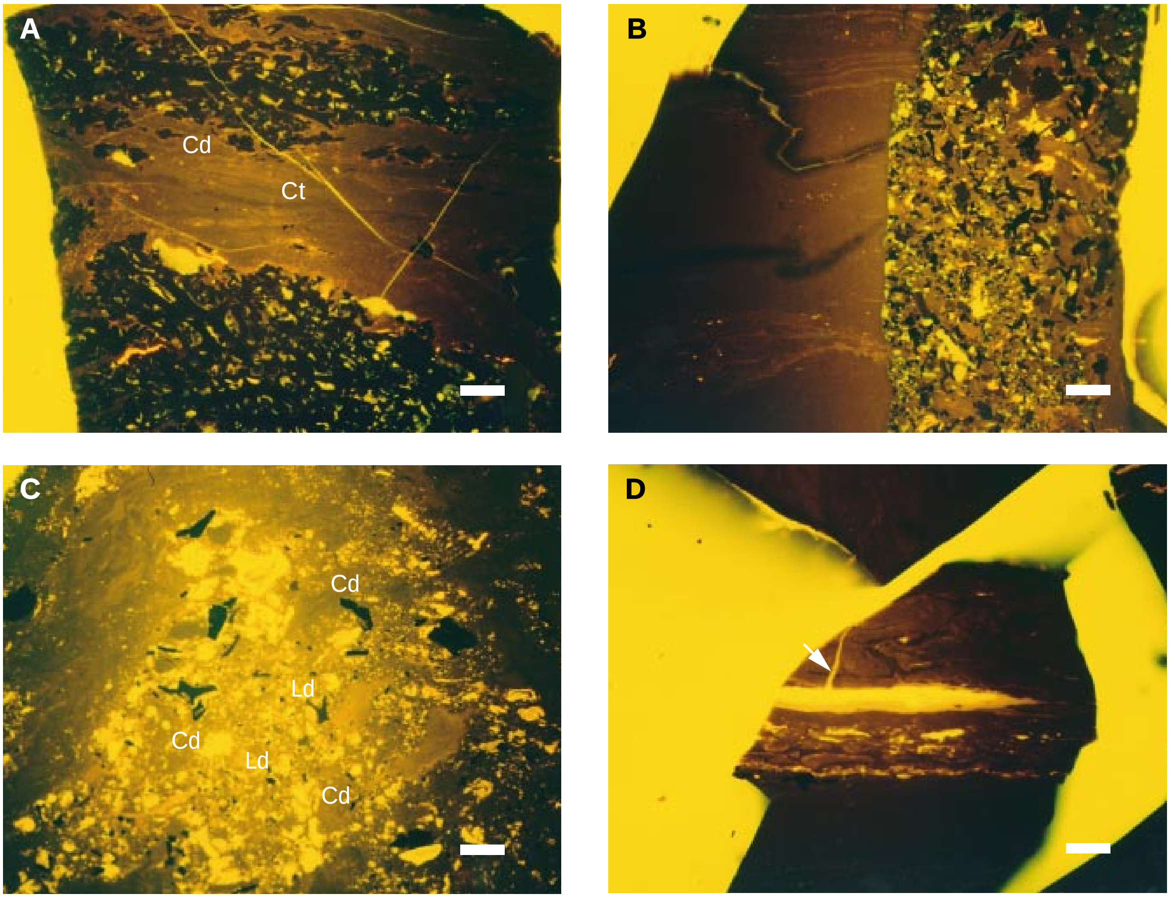

Fig. 25. Photomicrographs from seam T3 in the West Lulu-1 well. **A**: Contact between non-fluorescent inertodetrinite and macrinite (dark particles), and fluorescent collodetrinite (Cd) and collotelinite (Ct) (sample 4475A, 0–5.08 cm). **B**: Contact between fluorescent collotelinite with thin cutinites (left) and a mixture of fluorescent collodetrinite and liptodetrinite and non-fluorescent inertodetrinite (right). Note the lowered fluorescence intensity due to oxidation along cleats in the collotelinite (sample 4473A, 17.78–25.40 cm). **C**: Mainly liptodetrinite (Ld) in groundmass of fluorescent collodetrinite (Cd) (sample 4473A, 17.78–25.40 cm). **D**: Exsudatinite expelled into small cleat (arrow) (sample 4473A, sample 17.78–25.40 cm). All photographs in reflected light, blue-light irradiation and water immersion. Scale bar ~ 30 µm.

observed (Fig. 25). Pyrite varies between 0.2 and 1.8 vol.% and the content of detrital minerals amounts to 6.0 vol.% (carbominerite: 19.0 vol.%).

Seam T4. In West Lulu-1 the seam is characterised by an increasing content of vitrinite and vitrite+clarite and a contemporaneous decrease in inertinite and vitrinertite+durite+clarodurite and inertite from base to top (Figs 19, 26). The vitrinite is strongly fluorescent, and the inertodetrinite is generally fine-grained and allochthonous. Minute and framboidal pyrite is present.

Except for an interval dominated by inertinite and inertinite-rich microlithotypes in approximately the middle part of T4 in Lulu-1, the seam is also in this well characterised by high contents of vitrinite, generally fluorescent, and vitrite+clarite (Figs 19, 26). The inertinite in the inertinite-rich interval is composed of high-reflecting pyrofusinite, semifusinite, macrinite and fine-grained, relatively well-sorted inertodetrinite commonly associated with liptinite. Char is observed in the uppermost part of the seam (see Petersen 1998). Detrital mineral matter does not exceed 1.6 vol.% in the majority of the seam. However, in the uppermost part it increases to 6.6 vol.% (carbominerite 29.0 vol.%). Likewise the pyrite content, part of which is framboidal, increases to 4.2 vol.%. Liptodetrinite, sporinite, cutinite and resi-

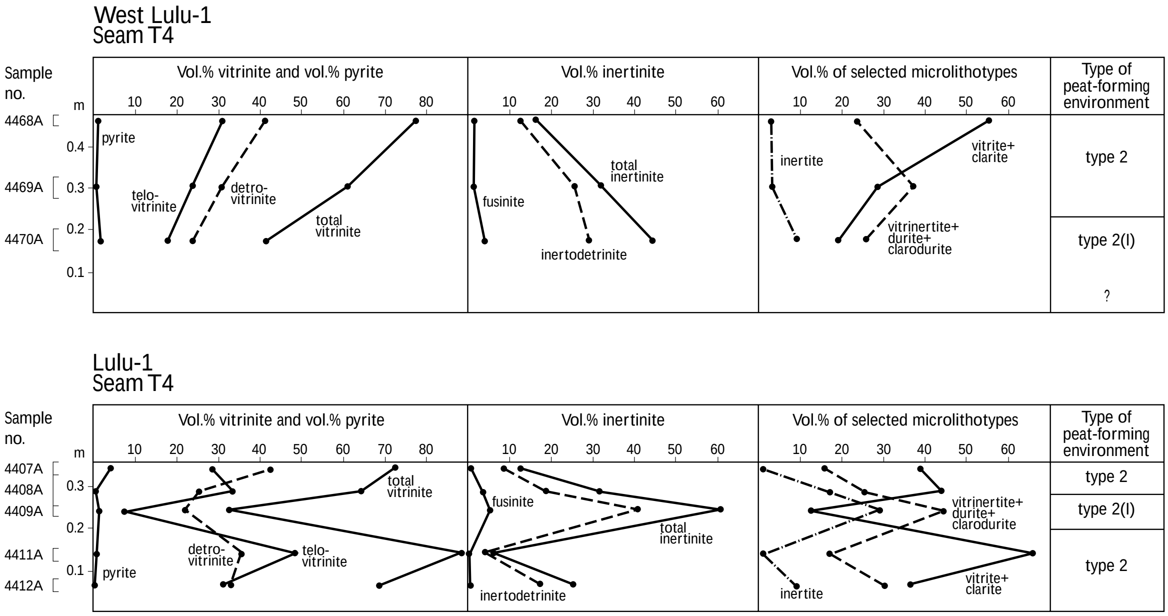

Fig. 26. Coal petrographic composition of seam T4 in the West Lulu-1 and Lulu-1 wells.

nite constitute the liptinite maceral group throughout the seam in both wells, and the content lies between 1.8 and 7.0 vol.%. The highest content of a single liptinite maceral is 4.2 vol.% (liptodetrinite, sample 4470, West Lulu-1), but in general individual liptinite macerals constitute not much more than 1 vol.%.

In Amalie-1 well T4 is again dominated by vitrinite (76.6–88.0 vol.%) and vitrite+clarite (59.8–61.0 vol.%) (Fig. 19). Char and pyrolytic carbon have been observed. Due to the high rank of the coal in this well, and thus the absence or only very weak fluorescence of the liptinite macerals, the liptinites could only occasionally be distinguished.

Mudstones. Four coaly mudstone or thin coal laminae samples from the West Lulu-3 and West Lulu-1 wells reveal an organic petrographic composition very similar to the main coal seams. The vitrinite maceral group dominates (41–86 vol.%) followed by the inertinite maceral group (8–29 vol.%). The liptinite content varies from 5 to 11 vol.%. Carbominerite, vitrite, duroclarite and vitrinertite are the primary microlithotypes.

Screening data

West Lulu-3. A total of 29 coal and coaly mudstone samples were analysed (Fig. 6). T_{max} values range between 439°C and 447°C and average 444°C (Fig. 27). Four extracted coal samples do not provide a change in the T_{max} values compared to the untreated counterparts. In the 20 coal samples hydrogen index (HI) values range between 118 and 331 (average: 178), but with the majority below 200 (Fig. 27). The HI values range between 128 and 211, average 172, in the coaly mudstone samples. In this well coal seam R1 has the highest average HI value and the highest average thermal extracted and generated petroleum content, S_1+S_2 = 140.45 mg HC/g rock (Table 11). The sample with a HI = 331 has a S_1+S_2 content of 253.84 mg HC/g rock, which is considerably above the average, and the content thus has a strong influence on the average S_1+S_2 value of seam R1.

West Lulu-1. A total of 44 coal and coaly mudstone samples were analysed (Table 5). The T_{max} values range between 436°C and 446°C and average 440°C (Fig. 27). No change in the T_{max} values is observed during pyrolysis of extracted samples. The HI values range between 126 and 242 in 38 coal samples and between 142 and 195 in 6 coaly mudstone samples averaging 180 and 168 respectively (Fig. 27). The highest average HI values on the basis of individual seams is found in seams T2, T3 and T4, with an average HI of 222 in seam T3 as the maximum, and the lowest values in seams R1a and R1 (Table 11).

Average thermal extracted and generated petroleum contents, S_1+S_2, are likewise highest in seam T3 (164.11 mg HC/g rock) and lowest in seam R1 (122.85 mg HC/g rock) (Table 11).

Fig. 27. Hydrogen Index vs. T_{max} plot of coal and coaly mudstone samples from the West Lulu-3, West Lulu-1, Lulu-1 and Amalie-1 wells. The samples plot within the band of typical kerogen type III. Note a tendency to higher HI values from West Lulu-3, over West Lulu-1 to Lulu-1, and the overlap of the coal and coaly mudstone samples. The lower HI values obtained from the Amalie-1 samples are caused by the higher maturity of the organic matter (%R_m = 1.3). ●: coal; ▲: coaly mudstone.

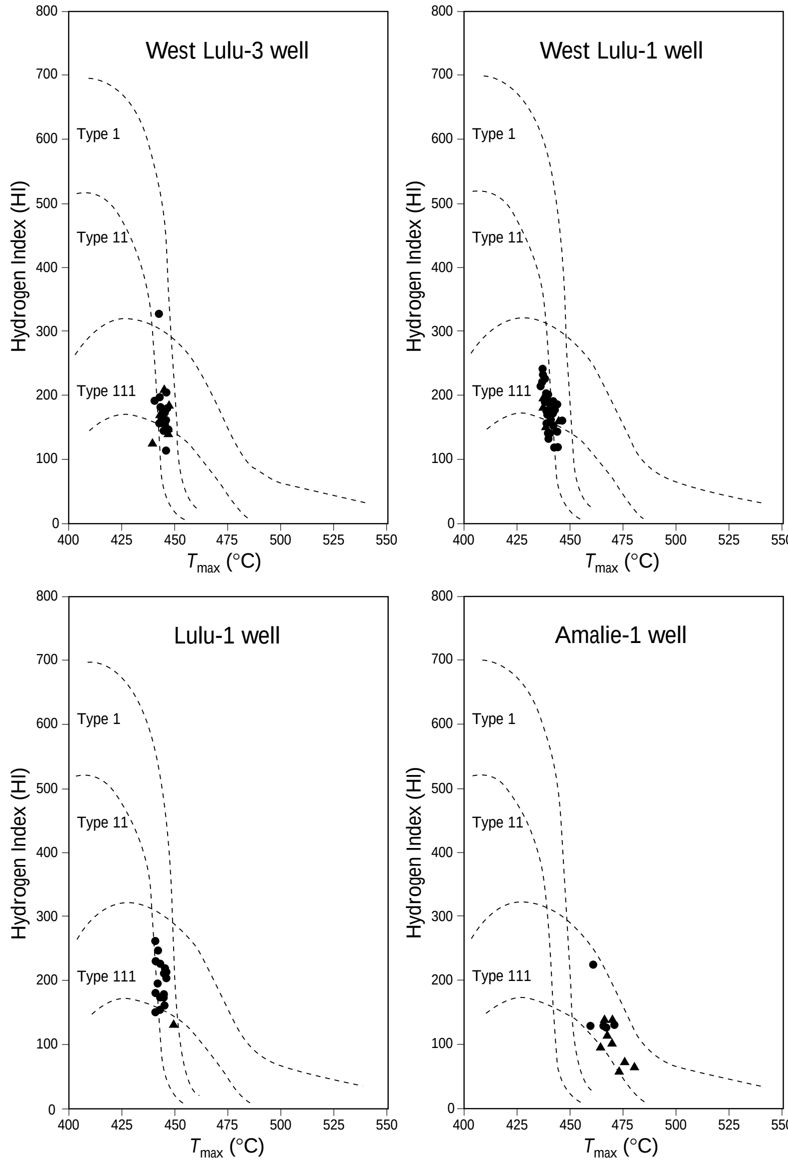

Lulu-1 well. A total of 16 coal samples and 2 coaly mudstone samples were analysed (Fig. 8). The T_{max} ranges between 440°C and 449°C with an average of 443°C (Fig. 27). Extracted samples and their untreated counterparts show more or less similar T_{max} values. In the coal samples HI varies between 152 and 263, averaging 200, and in the 2 coaly mudstones HI is 133 and 157. Seam T4 has the highest average HI (HI = 222) in this well (Table 11). Seam T2 gives the highest average thermal extracted and generated petroleum contents, S_1+S_2 = 163.19 mg HC/g rock, and seam R1 the lowest value (143.24 mg HC/g rock) (Table 11).

Amalie-1 well. Five coal samples and 8 coaly mudstone samples were analysed in this well (Fig. 9). The T_{max} varies between 459°C and 480°C with an average of 468°C (Fig. 27). The T_{max} value of an extracted sample is very similar to the untreated counterpart. The HI lies between 129 and 225 in the coal samples and between 60 and 140 in the coaly mudstones, averaging 149 and 99 respectively (Fig. 27). The highest HI value of 225 is derived from a thin coal layer not related to one of the established seams. Seam T4 has the highest average thermal extracted and generated petroleum content of all seams in the Amalie-1 well (Table 11).

Table 11. Average Hydrogen Index and average S_1+S_2 for the Bryne Formation coals

Well	Seam	Average Hydrogen Index (mg HC/g TOC)	Average S_1+S_2 (mg HC/g rock)
West Lulu-2*	T4	215	182.30
West Lulu-1	T4	217	152.59
Lulu-1	T4	222	159.62
Amalie-1	T4	131	110.84
West Lulu-2*	T3	203	181.49
West Lulu-1	T3	222	164.11
West Lulu-2*	R2	186	160.83
West Lulu-2*	T2	205	165.80
West Lulu-3	T2	167	129.94
West Lulu-1	T2	177	139.37
Lulu-1	T2	182	163.19
West Lulu-3	R1a	148	109.06
West Lulu-1	R1a	160	140.52
West Lulu-2*	R1	208	167.38
West Lulu-3	R1	194	140.45
West Lulu-1	R1	164	122.85
Lulu-1	R1	201	143.24
Amalie-1	R1	129	85.95

*data from Petersen *et al.* (1996)

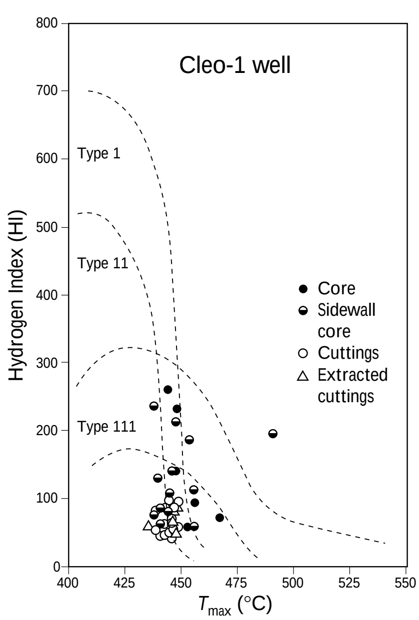

Fig. 28. Hydrogen Index vs. T_{max} plot of core samples, sidewall core samples, cuttings and extracted cuttings from the Cleo-1 well. The majority of the samples show low HI values corresponding to kerogen type IV.

Table 12. Cleo-1 well: screening data

Sample type	Depth (m)	TOC (wt%)	T_{max} (°C)	S_1 (mg HC/g rock)	S_2 (mg HC/g rock)	HI	PI
Core	4602.84	72.16	443	6.33	186.68	259	0.03
	4603.14	3.21	452	0.37	1.84	57	0.17
	4603.57	72.06	447	6.90	165.40	230	0.04
	4605.78	2.73	467	0.35	1.90	70	0.16
	4608.53	2.57	456	0.26	2.40	93	0.10
	4609.74	3.55	447	0.33	4.90	138	0.06
SWC	4551	28.50	447	6.56	60.11	211	0.10
	4553	62.90	437	19.14	147.81	235	0.11
	4554	31.89	490	3.83	60.63	190	0.06
	4563	0.73	437	0.14	0.55	75	0.20
	4572	5.40	439	1.34	6.94	129	0.16
	4579	0.60	440	0.11	0.37	62	0.23
	4605	0.69	443	0.13	0.56	81	0.19
	4607	0.43	453	0.33	0.79	184	0.29
	4615	0.40	440	0.10	0.34	85	0.23
	4639	1.30	455	0.14	0.76	58	0.16
	4641	1.37	444	0.25	1.47	107	0.15
	4654	11.63	455	2.40	13.03	112	0.16
	4660	2.98	445	1.10	4.17	140	0.21
Cuttings	4563	1.37	444	0.15	0.69	50	0.18
	4572	2.20	446	0.47	1.89	86	0.20
	4581	1.58	444	0.32	1.10	70	0.23
	4590	1.50	442	0.32	0.95	63	0.25
	4599	1.06	442	0.24	0.91	86	0.21
	4609	2.44	444	0.46	2.36	97	0.16
	4618	1.18	443	0.21	1.02	86	0.17
	4627	1.55	448	0.30	1.45	94	0.17
	4636	1.18	445	0.22	0.80	68	0.22
	4645	0.91	447	0.10	0.50	55	0.17
	4654	1.69	448	0.31	0.98	58	0.24
	4663	0.55	445	0.16	0.35	64	0.31
	4673	0.50	438	0.12	0.26	52	0.32
	4682	0.62	438	0.33	0.50	81	0.40
	4691	0.65	440	0.20	0.29	45	0.41
	4700	0.40	441	0.07	0.24	60	0.23
	4709	1.10	442	0.20	0.50	45	0.29
Extracted cuttings	4554	3.05	448	0.12	2.65	87	0.04
	4584	0.88	445	0.04	0.42	48	0.09
	4621	2.15	445	0.12	1.77	82	0.06
	4657	1.32	446	0.07	0.87	66	0.07
	4694	1.25	435	0.06	0.74	59	0.07

Cleo-1 well. Two vitrinite lenses (twigs ?) and 4 coaly mudstone samples from the cored interval were analysed (Fig. 10). T_{max} values from the core samples range between 443°C and 467°C with the lowest values obtained from vitrinite lenses (Fig. 28; Table 12). The vitrinite lenses show comparatively high HI values, 259 and 230, whereas the coaly mudstones give HI values between 57 and 138. An additional 13 side wall cores, 18 cuttings and 5 extracted cuttings derived from *c.* 4551–4709 m depth are shown in Figure 28 and in Table 12. Seventy-five per cent of the samples exhibit T_{max} values between 440°C and 448°C, whereas the HI values for all samples varies between 39 and 235 with the majority below 100.

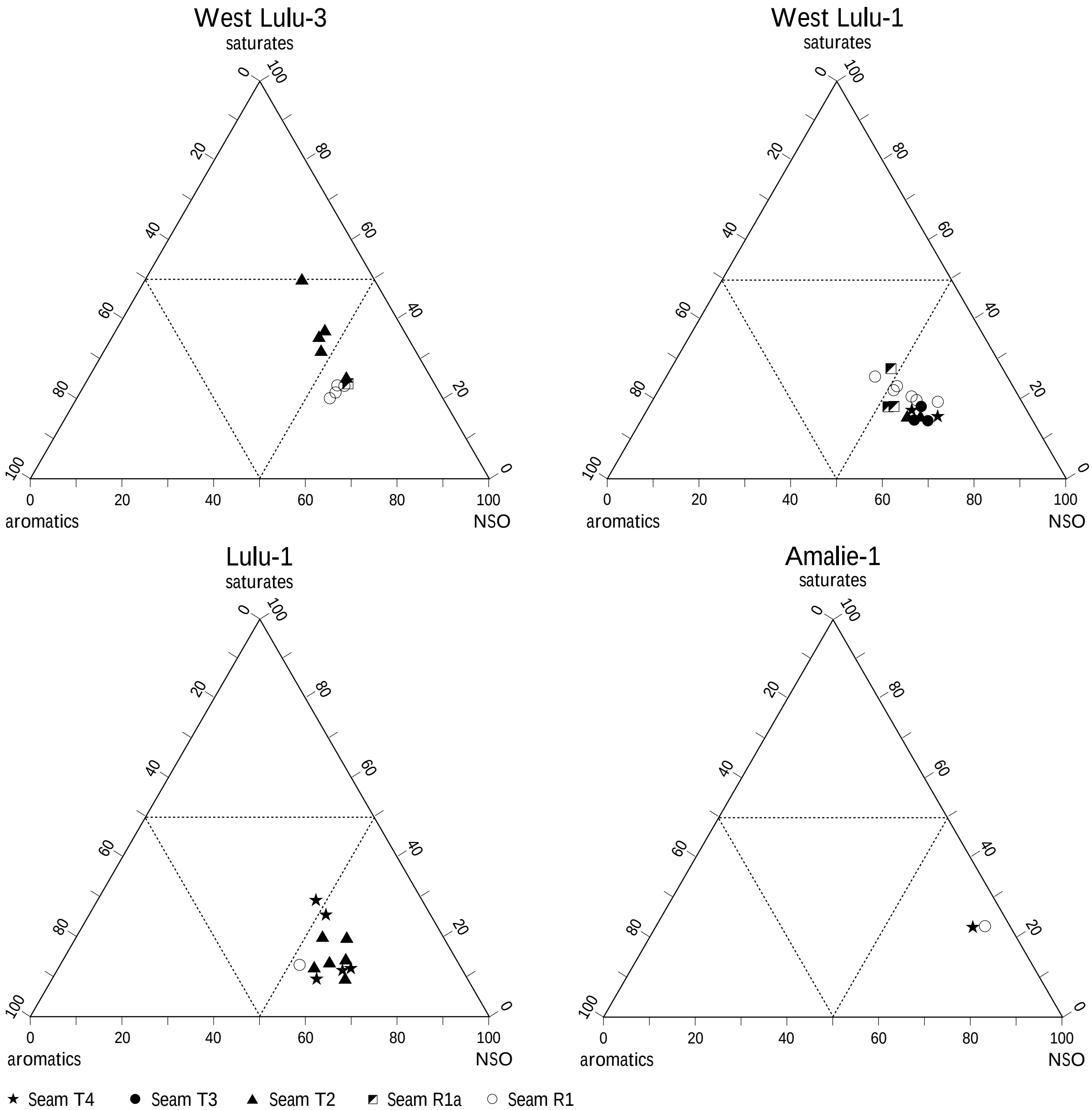

Fig. 29. Composition of the asphaltene-free solvent extract fraction from samples from coal seams R1, R1a, T2, T3 and T4 in the West Lulu-3, West Lulu-1, Lulu-1 and Amalie-1 wells. The extract fractions show dominance of NSO compounds.

Extracts

A total of 12 samples in West Lulu-3, 18 samples in West Lulu-1, 12 samples in Lulu-1 and 6 samples in Amalie-1 were extracted for further detailed organic geochemical analyses. The extracts from both coal and coaly mudstone samples in all the wells are dominated by NSO compounds which in general exceed 50% (Fig. 29). In the West Lulu-1 and Lulu-1 wells aromatic compounds are second and generally exceed 22%. This picture is different from the West Lulu-3 extracts where in only a few cases do the aromatic compounds exceed 22%, whereas the saturates in general constitute more than 23%. Four of the extracts from Amalie-1 likewise have a higher content of saturates, in particular in extracts from the coal samples. A single extract (4609.74 m) from Cleo-1 is dominated by NSO compounds (79.7%) followed by saturates (11.6%) and aromatics (8.7%).

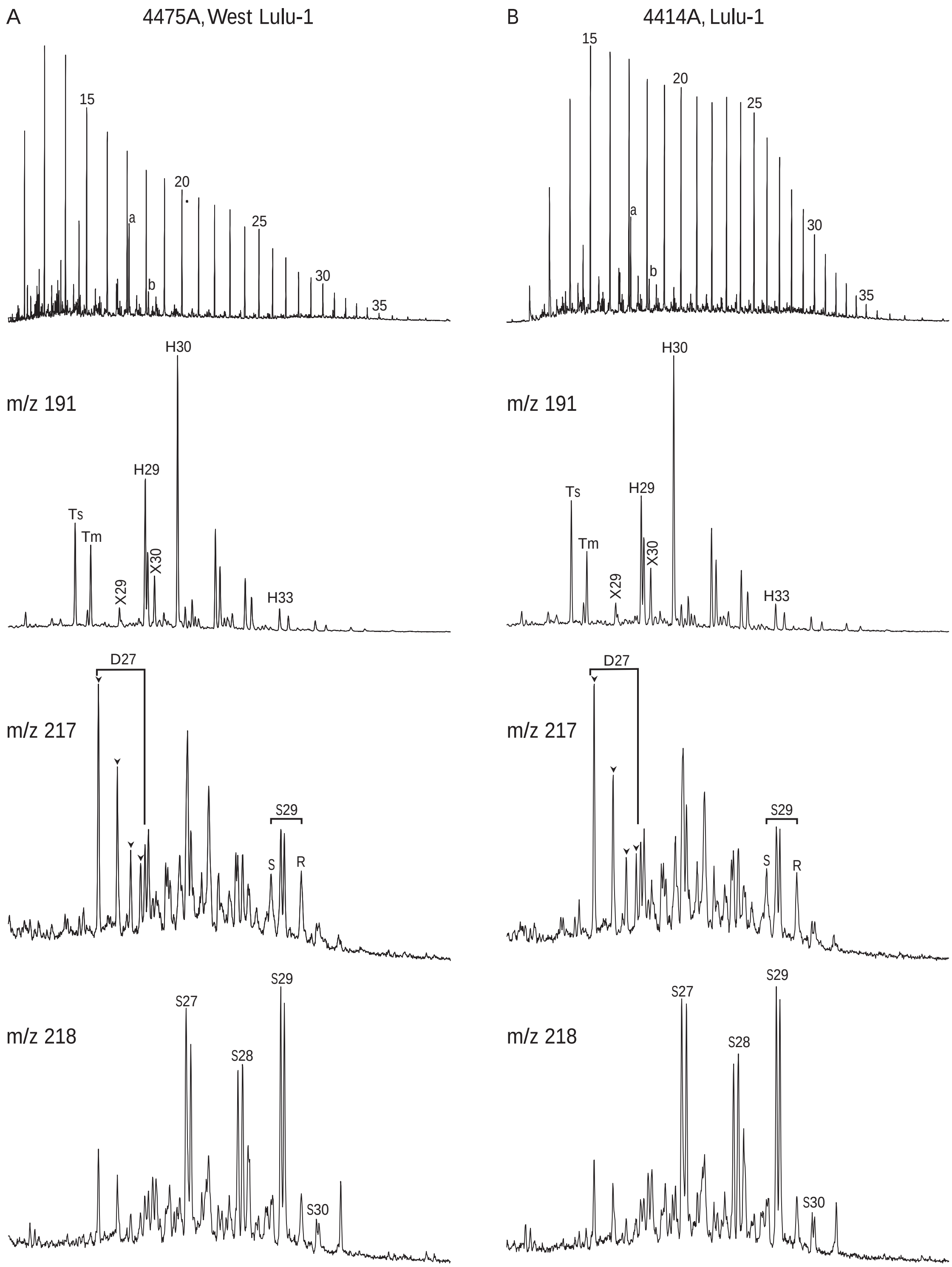

Fig. 30. Examples of gas chromatograms and m/z 191, m/z 217 and m/z 218 ion fragmentograms from saturated fractions of solvent extracts of Bryne Formation coals. **A**: sample 4475A, seam T3, West Lulu-1 well; **B**: sample 4414A, seam T2, Lulu-1 well. Annotation: numbers on GC-traces refer to *n*-alkane carbon numbers, a: pristane, b: phytane; Ts: trisnorneohopane, Tm: trisnorhopane, H29: norhopane, H30: hopane, H33, trishomohopane, X29: dianorhopane, X30: diahopane; D27: C_{27} diasteranes (4 isomers), S27, S28, S29 and S30: $C_{27-30}\alpha\beta\beta$ regular steranes, S: $C_{29}\alpha\alpha\alpha$(20S), R: $C_{29}\alpha\alpha\alpha$(20R). Note the high proportions of C_{27} steranes and the presence of C_{30} steranes indicative of marine influence during deposition.

Gas chromatography

The typical GC trace of the saturated fraction is characterised by a light-end-biased *n*-alkane distribution and a predominance of the nC_{14} to nC_{17} range (Fig. 30). The pristane/phytane ratios (Pr/Ph) are in general higher than 2.5 for all samples, but differences between wells are observed. The highest Pr/Ph ratios are present in the West Lulu-3 well, where the ratios range between 5.19 and 7.77, averaging 5.98, with the highest values occurring in the coaly mudstones (Tables 7–10). These high values are comparable to the values obtained in seams R1 and R2 in West Lulu-2 (Petersen *et al.* 1996). The Pr/Ph ratios decrease in a seaward direction and average 3.47 in West Lulu-1, 2.88 in Lulu-1 and 2.55 in Amalie-1. The carbon preference index (CPI) calculated from $2(C_{23}+C_{25}+C_{27}+C_{29})/[C_{22}+2(C_{24}+C_{26}+C_{28})+C_{30}]$ in any sample never exceeds 1.15 and is close to 1 for all samples from the wells (Tables 7–10).

In the Cleo-1 well, the Pr/Ph ratio is 1.57 and the CPI is 1.07 (Table 13).

Table 13. Cleo-1 well: GC data and composition of solvent extract fraction (asphaltene-free)

Depth (m)	Pr/Ph	CPI	EOM	Sat (%)	Aro (%)	Polars (%)
4609.74	1.57	1.07	25	12	9	79

Table 14. Average of C_{35}-homohopane index

Well / Seam	W. Lulu-3	W. Lulu-1	Lulu-1	Amalie-1
T4	-	0.023	0.037	0.034
T3	-	0.021	-	-
T2	0.016	0.020	0.034	-
R1a	0.012	0.016	-	-
R1	0.011	0.013	0.020	0.045
Mudstones	0.010	0.013	-	0.047
Average*	0.013	0.017	0.034	0.044

*average of coals and mudstones

Gas chromatography/mass spectrometry

Pentacyclic triterpanes. The distribution of the hopanes is dominated by the regular hopanes, with a maximum at C_{30}, and with the concentration of extended hopanes decreasing with increasing carbon number (Fig. 30). The 22S/(22S+22R) epimer ratios of the 17α(H),21β(H) C_{31}–C_{35} extended hopanes range between 0.57 and 0.67, with the majority around 0.60. The 'C_{35}-homohopane index', defined as $C_{35}/\Sigma C_{31-35}$ (Peters & Moldowan 1991), varies between wells and seams and laterally within seams (Table 14). Even though these differences are rather small a consistent landward–seaward trend is present in the data. The most landward wells, West Lulu-3 and West Lulu-1, relative to the palaeo-shoreline, have average indices (coal seams and mudstones) of 0.013 and 0.017 respectively, whereas the Lulu-1 and Amalie-1 wells situated seaward have average indices of 0.034 and 0.044 respectively. Individual seams likewise show increasing ratio in a seaward direction, e.g. the index increases from 0.011 to 0.045 in seam R1. Except for Amalie-1, seams T2, T3 and T4 have higher indices than seams R1 and R1a.

In the Lulu-1 and Amalie-1 wells 28,30-bisnorhopane is present.

Epimer ratios of C_{31}–C_{35} extended hopanes lie between 0.56 and 0.63 in the single sample from the Cleo-1 well, and the C_{35}-homohopane index is 0.028.

Steranes. With the exception of an outlier of 0.25, the ααα20S/(20S+20R) epimer ratios of the C_{29} steranes range between 0.36 and 0.51, with the majority lying between 0.45 and 0.50 (Tables 7–10). The range of the αββ20(S+R)/[αββ20(S+R)+ααα20(S+R)] ratio is between 0.44 and 0.66, except for an outlier of 0.37, but the majority (73%) lie between 0.50 and 0.64 (Tables 7–10).

The relative proportions of C_{27}αββ, C_{28}αββ and C_{29}αββ compared to the total amounts of the three steranes are shown in Figure 31 and Tables 7–10. The coals of the West Lulu-3 well are characterised by the highest contents of C_{29} sterane and the lowest contents of C_{27} sterane averaging 59.2% and 15.0% respectively. In the coals of the West Lulu-1 well the C_{29} sterane content has fallen to an average of 45.2% and the C_{27} sterane content has increased to an average of 27.0% (Fig. 31). These trends are continued in the coals of the Lulu-1 and Amalie-1 wells where the average C_{29} sterane content has decreased to 38.0% and 35.8% respectively and the average C_{27} sterane content has increased to 33.5% and 35.8% respectively (Fig. 31). Thus, generally the average content of C_{29} steranes in a well decrease and that of C_{27} steranes increase in a seaward direction, and this is also valid within a seam if it is followed laterally in a landward–seaward direction (e.g. seam R1, Fig. 31; Tables 7–10). Furthermore, it is evident that T-seams (seams T2, T3 or T4) compared to R-seams (seams R1 and R1a) in a well generally have a higher content of

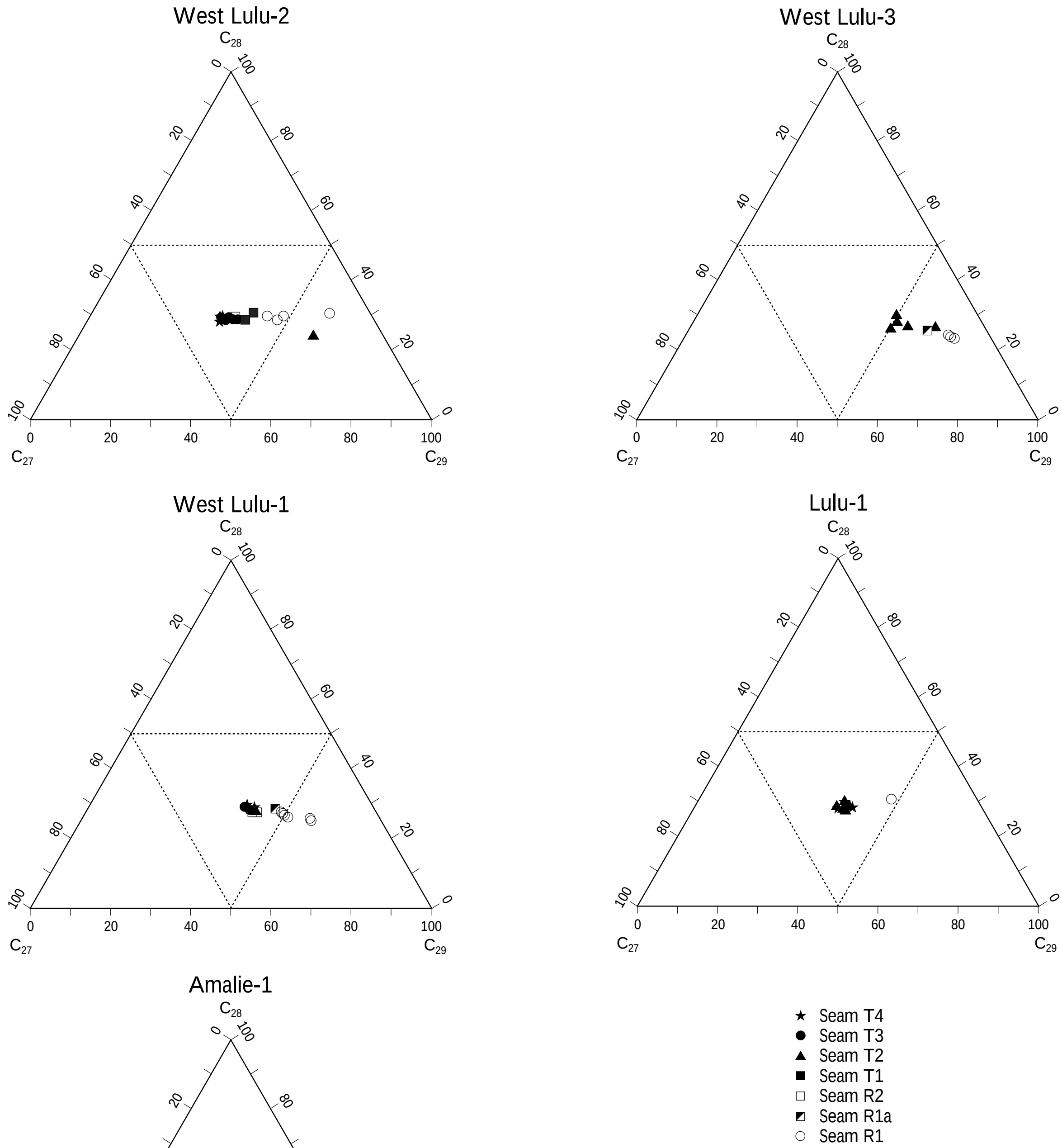

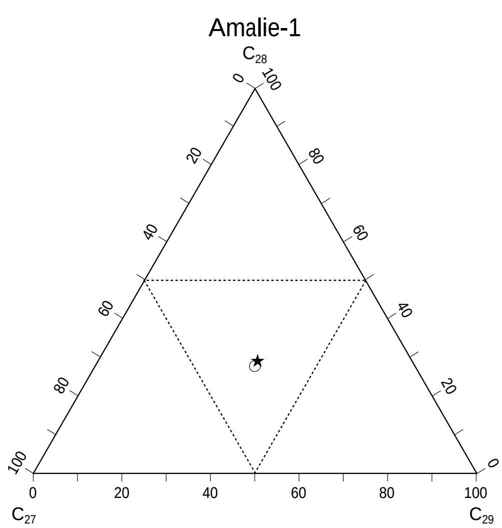

Fig. 31. Normalised $C_{27–29}$ sterane distribution in samples from coal seams R1, R1a, R2, T1, T2, T3 and T4 in the West Lulu-3, West Lulu-2 (data from Petersen *et al.* 1996), West Lulu-1, Lulu-1 and Amalie-1 wells. In general the T-seams formed during an accelerated relative sea-level rise contain a higher proportion of C_{27} sterane. This suggests increased marine influence on the mires during peat deposition compared to the precursor peats of the R-seams.

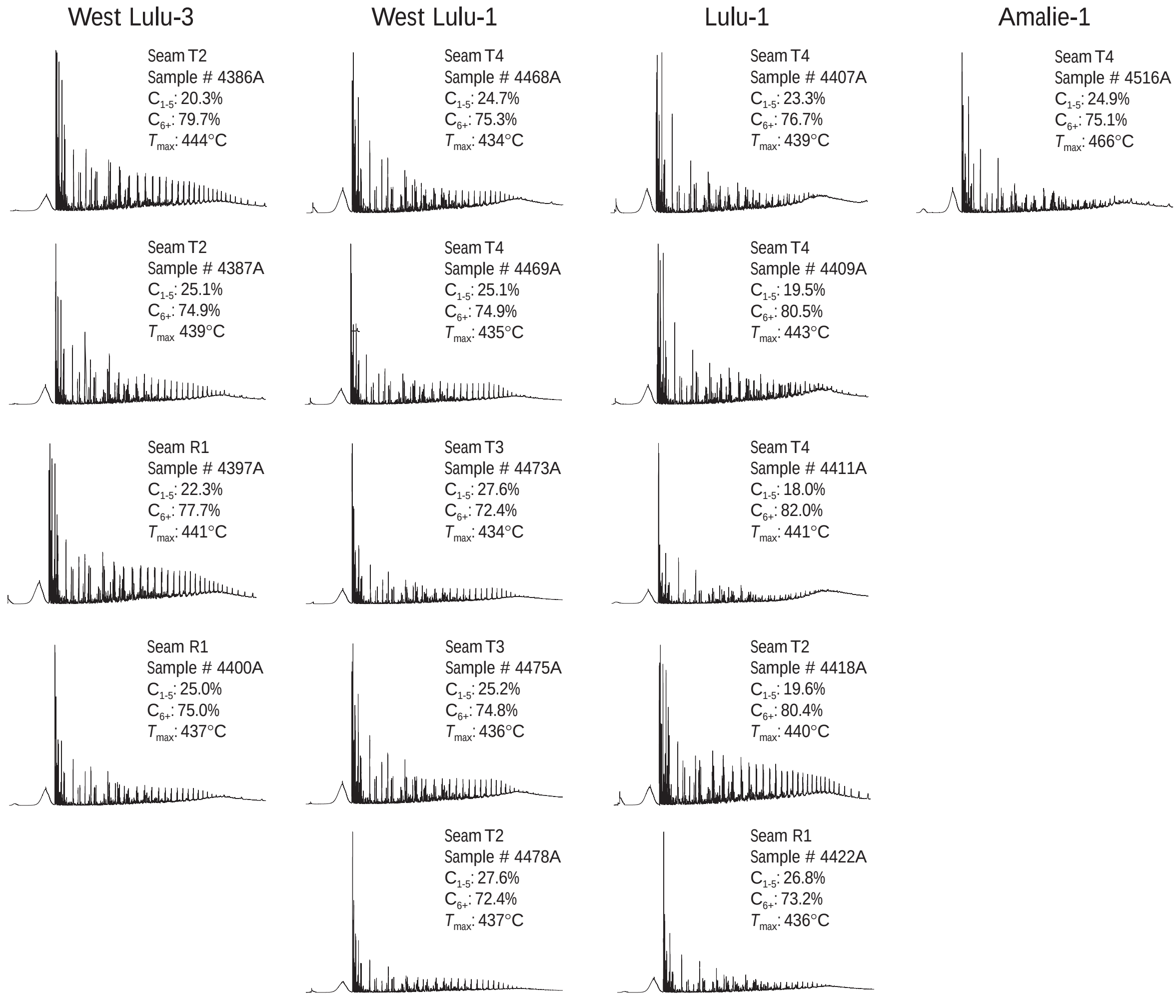

Fig. 32. Pyrograms of the 15 solvent-extracted coal samples from four wells in the Søgne Basin. The pyrolysates are characterised by low molecular weight aromatic/phenolic compounds and normal alkanes/alkenes.

C_{27} steranes. However, this difference diminishes in a seaward direction as shown in the Amalie-1 well (Fig. 31; Table 10).

The ααα20S/(20S+20R) epimer ratio of the C_{29} steranes in the Cleo-1 well sample is 0.44, while the αββ20(S+R)/[αββ20(S+R)+ααα20(S+R)] ratio is 0.53. The distribution of the C_{27}, C_{28} and C_{29} regular steranes are 11%, 23% and 66% respectively.

Pyrolysis-gas chromatography

A total of 15 coal samples were selected from the West Lulu-3, West Lulu-1, Lulu-1 and Amalie-1 wells. The sample set thus represents a landward (West Lulu-3) to seaward (Amalie-1) transect with respect to the palaeoshoreline. The samples were selected from seams R1 (West Lulu-3 and Lulu-1 wells), T2 (West Lulu-3, West Lulu-1, Lulu-1 wells), T3 (West Lulu-1 well), and T4 (West Lulu-1, Lulu-1, and Amalie-1 wells). Pyrograms of the samples are shown in Figure 32. Generally, the overall pyrolysate composition is very similar for all samples, but minor differences between individual seams may be detected in the detailed pyrolysate compositions. Except for sample 4397A from West Lulu-3, pyrolysates of seam R1 show very modest proportions of unresolved components, and prominence of a number of low molecular weight aromatic/phenolic compounds, notably benzene, alkyl-benzenes, phenol, alkyl-phenols, naphthalene, alkyl-naphthalenes, and 'unknowns' compared to normal alkanes/alkenes. Normal alkanes/alkenes are present at least up to chain-lengths of 26 carbon atoms. Sample 4397A, which was collected close to the top of seam R1, shows some resemblance to samples of the overlying seam T2. T2 samples generally yield higher proportions of *n*-alkanes/alkenes, which may be present up to chain lengths of at least 35 carbon atoms, and a minor envelope of unresolved components centred around nC_{25}. Aromatic and phenolic moieties are of minor importance compared to *n*-alkyl moieties. Samples of seam T3, which was sampled only in the West Lulu-1 well, are somewhat depleted in *n*-alkyl moieties compared to the T2 samples discussed above, both with respect to abundance relative to other resolved components, and with respect to maximum chain-length. This is even more pronounced in samples of seam T4.

Although *n*-alkyl components are prominent in a number of samples, aromatic/phenolic moieties and 'unknowns' tend to predominate. In particular, this is observed in the sample collected from the Amalie-1 well, which is of higher rank or maturity compared to the remainder of the samples. Higher rank/maturity will tend to increase the proportion of aromatic and phenolic moieties.

Results of the multivariate regression analysis

The multivariate regression analysis was carried out in order to create a model explaining as high a proportion of the variation of S_2 as possible. A model explaining 87% of the variation of S_2 was created, but includes only 51 out of 94 samples (= objects) (Fig. 33, class A). The following 19 variables are regarded as important to the variation of S_2: TOC, vitrinite (Vit), vitrite (V), clarite (Cl), duroclarite (DC), clarodurite (CD), carbominerite (CM), telinite (Tel), collotelinite (Collotel), collodetrinite (Collodetr), corpogelinite (Corpo), sporinite (Sp), cutinite (Cu), liptodetrinite (Lipto), resinite (Res), fusinite (Fus), semifusinite (Semif), inertodetrinite (Inerto) and macrinite (Mac). In contrast to an earlier model based only on data from West Lulu-2 (Petersen *et al.* 1996), the T_{max} values can be deleted from the model without any loss of information. Petersen *et al.* (1996) drew attention to the uncertainty by correlating T_{max} due to the small variance in maturity, and this fact may also be valid for the present data set which only shows limited variance in T_{max}. With a correlation coefficient of 0.94 and an average prediction error on S_2 of 11, the predictive ability of the model is good (Fig. 33, class A). The relatively low slope of 0.88 indicates, however, a lack in the models response, which implies that the petrographic composition together with the TOC values cannot fully explain the variation in S_2.

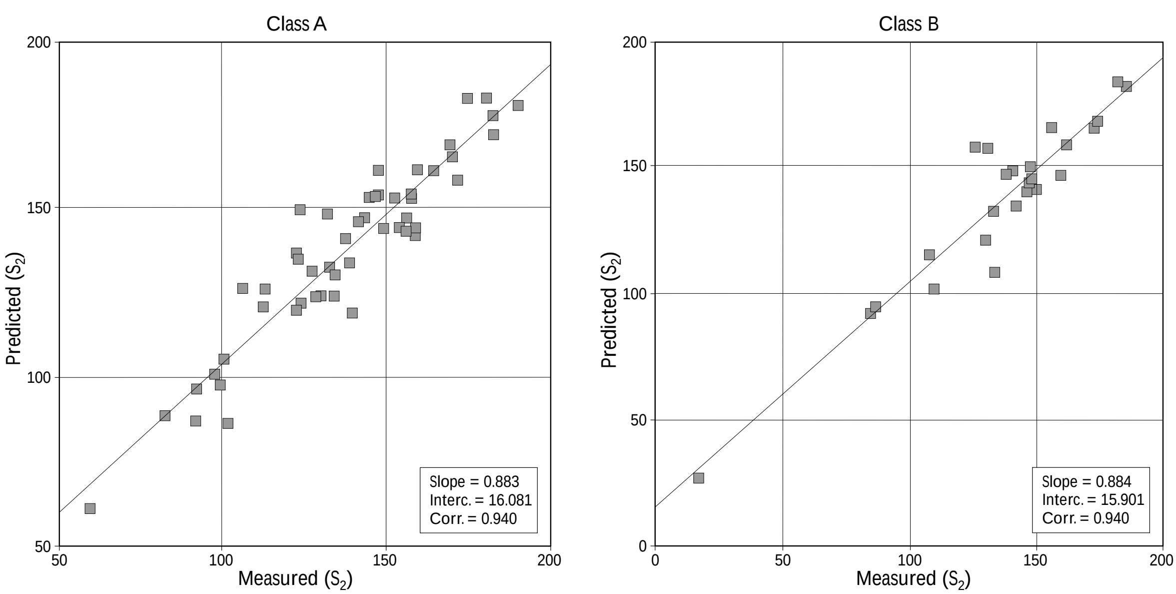

Fig. 33. Predicted vs. measured S_2 for classes A and B. The predicted values are responses from the partial least squares regresssion (PLSR) model. Correlations of 0.94 are considered to be reasonable, though slopes of 0.88 indicate a lack in the model's response.

Another model, comprising the same variables as the first model, was formed. This model included 26 of the remaining 43 samples. The predictive ability of this model is in the same order as the previous model (Fig. 33, class B), but with a somewhat higher (16) average prediction error. The difference between the two models was studied using SIMCA. The discrimination power of the individual variables indicates that the separation into two classes is primarily caused by duroclarite together with minor contributions from clarite, corpogelinite, cutinite and fusinite. Examination of the raw data did not reveal a clear trend in the dataset, which could satisfactory explain the separation into two classes. The bar graph shows the membership of individual samples to either class A or class B (Fig. 34). The samples exhibit a slightly higher membership to their own class than to the other class. The separation is however weak, and the separation into two classes cannot be justified from these results.

Consequently a third group was formed comprising the samples from classes A and B, with the same variables as used above. A few extra samples could be added to the combined group, ending with 81 of the 94 samples included in the model. The consequence of including more samples in the model is a weaker correlation, and only 71% of the variation in S_2 can be explained. The response is much weaker with a correlation coefficient of 0.85 and a slope of 0.73 (Fig. 35). The average prediction error is satisfactory at 14, but the variation in the prediction error is high. The general applicability of the model is, however much higher than for the previous two models, since more samples covering a wider span of variance are included. The low slope in the response line emphasises that other factors than the petrographic composition and the TOC values have significant influence on the S_2 value. Although the model appears to be relatively weak, it is possible to study the relations between the remaining petroleum generative potential and the petrographic characteristics, and it is possible to identify individual parameters with major influence on S_2, and those with little or no influence.

Samples not fitting the model were regarded as outliers. The raw data for the outliers were studied in order to explain why they did not fit the model. The outliers fell into two major groups: those having very high S_2 values and those having very low S_2 values. The first group comprises samples 291941, 291943, 291997 (Petersen & Andsbjerg 1996) and 4400A which all have S_2 values above 200. The second group comprises samples 291945, 291969, 291974, 4515A, 4516A and 4521A which have S_2 values around 100 or very low values.

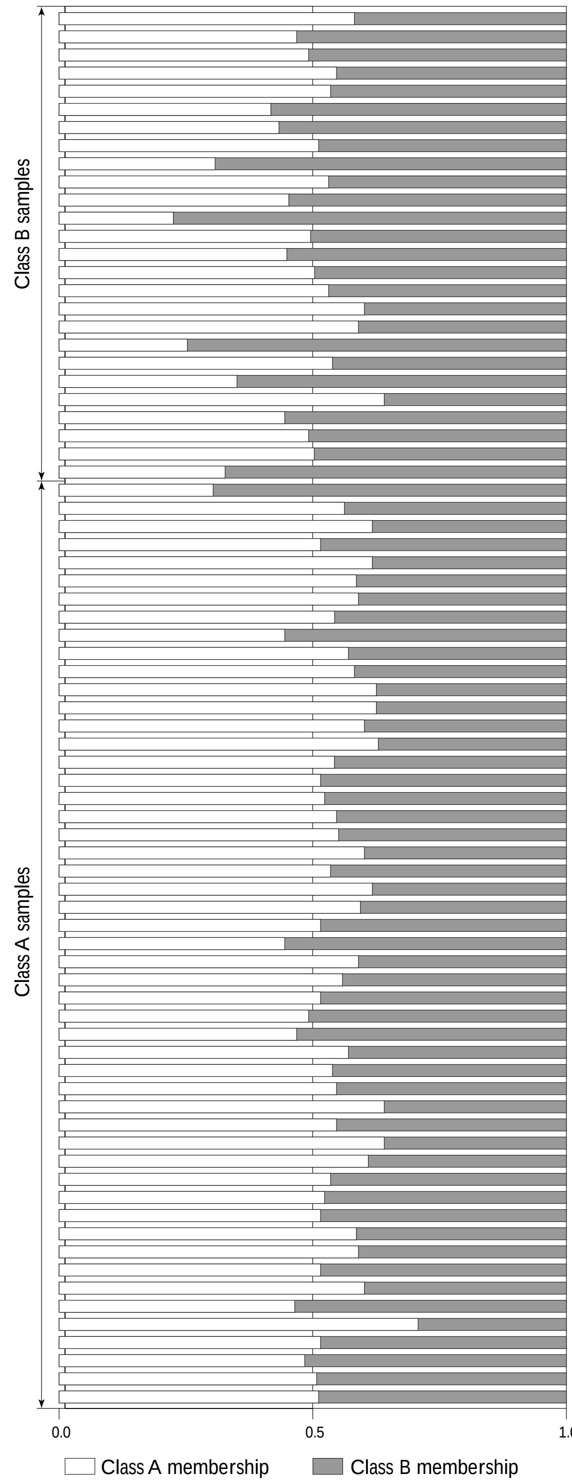

Fig. 34. Bar graph showing the individual sample's membership to either class A or class B. The samples exhibit a slightly higher membership to their own class; however, the separation is weak.

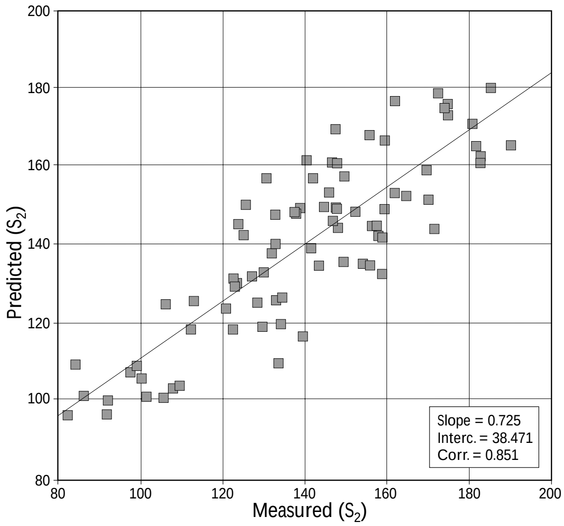

Fig. 35. Predicted vs. measured S_2 for the combined class comprising 81 samples of the 94 samples included in the model. The model explains 71% of the variation in S_2. Compared to class A and class B a weaker response is shown by a correlation coefficient of 0.85 and a slope of 0.73. The low slope of the response line emphasises that other factors than the petrographic composition and the TOC values have significant influence on S_2. However, the general applicability of the model is higher than for models A and B since more samples covering a wider span of variance are included.

It is likely that the inclusion of more samples with S_2 values in the low and high end would result in inclusion of the outliers in the model due to broadening of the models 'tolerance'.

Three other samples that do not fit the model are 4407A, 4487A and 4504A. Extreme S_2 values cannot explain these outliers, but some other 'extraordinary' characteristics compared to the samples fitting the model could be the reason: sample 4407A has an unusually low TOC value (48.24 wt%), sample 4487A has a relatively high clarite content (14 vol.%) together with a low inertinite content (9 vol.%), and finally 4504A has a high TOC value (80.1 wt%) combined with a relatively low S_2 value (101.4 mg HC/g rock).

Discussion

Peat-forming mires and depositional development of the coal-bearing succession

The types of mire environments indicated to the right on each coal seam log (Figs 18, 20, 21, 24, 26) is based on Petersen (1994). Type 1 is a wet, open mire represented by a limnic coal facies characterised by allochthonous organic components and a high content of allogenic inorganic components (> 20 vol.%). Type 2 is a low-lying, wet and generally anoxic mire, commonly isolated from active siliciclastic depositional systems, and represented by a vitrinite-rich coal facies formed by autochthonous peat accumulation. The vitrinite content is > 50 vol.%, the inertinite < 40 vol.% and the mineral content < 20 vol.%. The Type 2 mire is called Type 2(I) if considerable amounts of allochthonous, hypallochthonous or *in situ* formed pyroinertinite is present. The Type 3 mire environment is the driest of the three types and can be divided into two subenvironments, Type 3a and 3b. Both are represented by inertinite-rich coal facies: in Type 3a the vitrinite content is < 30 vol.% and the inertinite content > 60 vol.%, and in Type 3b the vitrinite content is between 30 and 50 vol.% and the inertinite content between 40 and 60 vol.%. These coal facies were formed due to a fluctuating watertable in the precursor mires, maybe associated with doming of the peat surface, which favoured periodic oxidation of the organic matter.

The siliciclastic sediments encasing the coal seams in the wells indicate that peat accumulation occurred in the vicinity of the palaeo-coastline in a coastal plain setting, and peat formation thus took place in coastal mires occasionally influenced by saline water (see below; Figs 6–9). The laterally extensive seam R1 is in the most landward position relative to the ancient shoreline overlying fluvial channel (West Lulu-3) and fluvial or tidal channel (West Lulu-2; Petersen & Andsbjerg 1996) deposits, and in a seaward direction shoreface or strandplain (West Lulu-1) and lagoonal (Lulu-1, Amalie-1) deposits. The seam represents in the four wells a wet type 2 mire environment characterised by high contents of vitrinite and fluctuating but generally high contents of vitrite+clarite (Fig. 18). However, although part of the inertinite in R1 in West Lulu-1 is composed of allochthonous inertodetrinite, a tendency to a decrease in the amount of vitrinite-rich microlithotypes coupled with an increase in inertinite-rich microlithotypes towards the top of the seam may suggest an incipient evolution towards drier conditions. The peat mire evolution at this location would thus be similar to the evolution observed in the West Lulu-2 well (Petersen & Andsbjerg 1996). Varying proportions of inertinite and inertinite-rich microlithotypes in R1 in West Lulu-3 may likewise be attributed to temporarily drier conditions, probably caused by an unstable watertable in the precursor mire. This is further supported by the

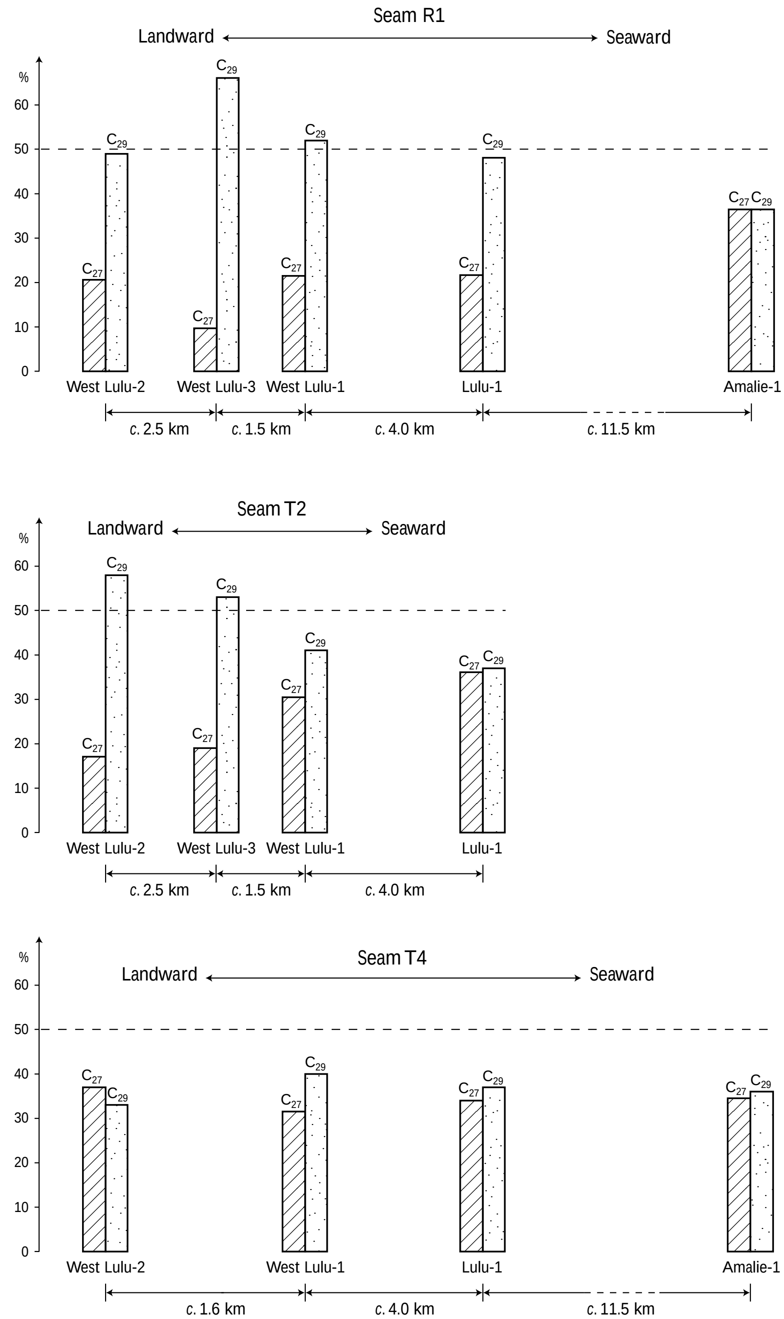

Fig. 36. Evolution in the proportion of steranes C_{27} and C_{29} in seams R1, T2 and T4 from a landward to a seaward position relative to the palaeo-coastline. A general decrease in the proportion of C_{29} sterane and associated increase in the proportion of C_{27} sterane towards the palaeo-shoreline in all three seams suggests stronger brackish–marine influence on the coastal reaches of the ancient mires. In addition, seams T2 and in particular T4 contain a higher proportion of C_{27} sterane than seam R1, indicating stronger brackish–marine influence on the precursor peat mires of seams T2 and T4.

presence of unsorted possibly oxidation-derived inertodetrinite and macrinite in the seam together with pyrolytic carbon, which may record ignition by lightning strikes, possibly exacerbated during drier periods. Pyrite, which may indicate a marine influence during peat formation (e.g. Cohen *et al.* 1984; Brown & Cohen 1995), is only present in low amounts or is absent indicating a mainly freshwater precursor mire of seam R1. This is also indicated by the predominance of C_{29} sterane (particularly in West Lulu-3), which is often attributed to terrestrial contributions to the organic matter (Huang & Meinschein 1979; Philp 1994), over C_{27} sterane, which is mainly related to marine algae (e.g. Hunt 1996; Figs 31, 36; Tables 7–10). Seaward, equal amounts are achieved in Amalie-1 (Fig. 36), although the higher maturity of the Amalie-1 coals may have influenced the sterane distribution (Dzou *et al.* 1995). Similarly the seam is, with the exception of Amalie-1, characterised by relatively lower C_{35}-homohopane indices than the other seams, in particular the T-seams (Table 14). The highest index is present in Amalie-1, i.e. in a seaward position. A high homohopane index is believed to indicate highly reducing marine conditions (Peters & Moldowan 1991). In a basinward direction, 28,30-bisnorhopane in seam R1 in Lulu-1 and Amalie-1 may also indicate marine-influenced anoxic conditions during peat deposition in this part of the precursor mire (e.g. Peters & Moldowan 1993).

Although a slight marine influence may be observed in a basinward direction the limited marine signature and prevailing 'terrestrial' nature of the seam composition is in good agreement with the interpretation of the depositional conditions for seam R1 in West Lulu-2 (Petersen & Andsbjerg 1996; Petersen *et al.* 1996). The seam marks the boundary between a lowstand systems tract or early transgressive systems tract and a transgressive systems tract, and peat-formation occurred during early relative sea-level rise and accordingly a low rate of base-level rise. In a landward direction a generally lower regional watertable may have favoured watertable fluctuations promoting both oxidation of the organic matter and wildfires. Seaward a continuously higher-standing watertable caused by a larger influence from the rise in relative sea-level diminished the influence from watertable fluctuations thereby reducing the amount of coal facies recorded in seam R1 in that area.

Continued watertable rise outpaced peat accumulation and in the location of Lulu-1 and Amalie-1 lagoonal conditions were established, whereas open-water mire and lake conditions were established more landward (Figs 6–9). However, presumedly a restricted watertable rise was not able to outpace the rate of peat accumulation at the position of West Lulu-2, where the precursor peat of seam R1 continued to accumulate peat. Peat formation was resumed in part of the previously flooded areas when conditions suitable for peat formation were re-established. This resulted in the split of seam R1, and the formation of seam R1a. Seam R1a carries many of the petrographic characteristics of seam R1, and in the position of West Lulu-1 the uppermost part of the seam accumulated in a type 3a mire environment characterised by an inertinite-rich coal facies (Fig. 20). Char particles derived from heat-effected, degassed humified organic matter (peat) and pyrolytic carbon, both indicative of wildfire, have been observed in R1a. In its organic geochemical composition R1a however, records an increased marine influence on the mire environment by having higher C_{27} sterane contents and C_{35}-homohopane indices than seam R1 (Fig. 31; Tables 7, 8, 14).

Following deposition of the laterally restricted seam R1a continued relative sea-level rise caused a regional rise in the watertable level resulting in formation of open-water mires and lakes, occasionally with deposition of splay sediments, in an area from West Lulu-2 seaward to Lulu-1 (Figs 6–9). Possibly a relative sea-level fall exposed the coastal plain, and a renewed base-level rise linked to a rise in relative sea-level created once again favourable conditions for peat accumulation due to a stagnant high standing watertable and sediment starvation over a large area. However, the transgressive sea hindered peat accumulation in the Amalie-1 area where lagoonal, estuarine channel, tidal flat, possibly lacustrine, shoreface and offshore deposition prevailed after deposition of seam R1 (Fig. 9). An open-water mire may, however, have been established temporarily (carbonaceous mudstone and thin coal, *c.* 5062 m on Fig. 9). It is possible that this level may be correlatable landward to one of the coal seams, but a correlation is not attempted on the basis of the available data.

According to Petersen & Andsbjerg (1996) the precursor peat of seam T2 accumulated during an accelerated rate of relative sea-level rise which resulted in a more 'wet' coal seam composition. Seam T2 in West Lulu-2 has a variable coal facies composition representing a rather complex succession of mire environment types, including the drier type 3b. This pattern is also seen in West Lulu-3 and West Lulu-1 (Fig. 21). In West Lulu-3 an increase in the content of inertinite and inertinite-rich microlithotypes up through the major part of the seam and a decrease in pyrite content towards the top suggests a freshwater mire with an unstable watertable, at least during deposition of the middle part (type 3b → type 2 → type 3b) of the coal seam. Char and oxidised cutinite and resinite are additional evidence for temporarily drier conditions. Likewise T2 in West Lulu-1 shows an evolution from a wet type 2 mire environment towards a dry type 3a mire characterised by a pronounced content of inertite. Allochthonous fine-grained and occasionally micrograded inertodetrinite, which may be associated with detrital liptinite, may characterise the coal facies of the type 2 mire environment. Such a coal facies with abundant inertodetrinite (well-sorted, rounded, micrograded, microlaminated) also characterises the inertinite-rich interval in T2 in Lulu-1 (Fig. 21), and represents a type 2(I) mire environment. The presence of char, fusinite and pyrolytic carbon points to an *in situ* wildfire-deriviation of part of the inertinite. Wildfires may lower the peat surface down to the groundwater table, which may promote redeposition of inertodetrinite and possibly the introduction of saline water (pyrite peak between 0.33–0.38 m in Lulu-1).

Despite the petrographic evidence for temporarily drier peat-forming conditions the nearly constant presence of pyrite, including framboidal forms, suggests that the T2 prescursor mire was generally wetter and more strongly influenced by the nearby sea than the precursor mires of both seams R1 and R1a. This would be in agreement with recent studies on the Changuinola peat deposit in Panama which suggests that coals with a distinct transgressive signature are likely to have a significant content of pyrite (Phillips & Bustin 1996). A more severe saline water influence on the T2 precursor mire is further indicated by the sterane distribution and the homohopane index (Fig. 31; Tables 7–9, 14). The relative proportion of C_{29} sterane is generally lower than in seams R1 and R1a and that of C_{27} sterane generally higher, and equal proportions are present in the Lulu-1 well (Fig. 36). Likewise, in a landward–seaward transect the homohopane index of seam T2 increases and in the wells it shows higher values than recorded in seams R1 and R1a. In the Lulu-1 position 28,30-bisnorhopane is also present in the coal.

A continued rise in relative sea-level caused drowning and transgression of the T2 precursor mire. The coastal reaches of the mire in the Lulu-1 area was transgressed by the sea and shoreface and offshore environments were established followed by shoreface and foreshore environments (Fig. 8). Landward, in the West Lulu-1 area, estuarine channels were established after peat mire termination (Fig. 7). Later lagoonal and flood tidal delta systems were formed. Further landward fluvial or tidal channels and bay-head deltas dominated (Fig. 6). The siliciclastic depositional systems thus reflect a marine transgression which reached the Lulu-1 area during maximum extent, whereas a diminished marine influence is recorded west of this area (West Lulu-1, West Lulu-2 and West Lulu-3) by sediments of marginal marine and paralic depositional systems.

In West Lulu-2, a *c.* 2 m thick coal bed was divided into two seams, R2 and T3, on the basis of organic petrography and geochemistry (Petersen & Andsbjerg 1996; Petersen *et al.* 1996). The R2 seam presumably has a very restricted areal extent and it has not been observed in the other wells. In West Lulu-2 seam T3 is characterised by a significant content of sulphur (average: 4.5%) which must reflect prolonged infiltration of saline water (Phillips *et al.* 1994). Seam T3 is present in West Lulu-1 and represents a wet type 2 mire environment (Fig. 24).The transgressive signature of T3 in this well is demonstrated by the presence of pyrite combined with high C_{27} sterane contents and a comparatively high homohopane index (Figs 24, 31; Tables 8, 14).

Peat accumulation in the precursor mire of seam T3 was terminated by deposition of siliciclastic sediments. Re-establishment of peat-forming conditions favoured deposition of seam T4 over a large area. The seam is present in all wells except West Lulu-3 (Fig. 12). In a landward–seaward transect from West Lulu-2 to Amalie-1 the seam is vitrinite- and vitrite+clarite-rich, and it represents a wet type 2 mire, occasionally enriched in fine-grained, allochthonous inertodetrinite or high-reflecting pyrofusinite (type 2(I) mire; Fig. 26). The pyrofusinite and char observed in Lulu-1 and Amalie-1, and in the latter also pyrolytic carbon, indicate that wildfires were active in the mire, probably mainly crown fires burning aerial plant tissues due to the generally high watertable suggested by the petrography. Framboidal and minute pyrite indicates marine influence during peat formation as does relatively high proportions of C_{27} sterane and homohopane indices (Fig. 31; Tables 8 –10, 14). Approximately equal proportions of C_{29} and C_{27} steranes occur in T4 seaward in Lulu-1 and Amalie-1 (Fig. 36), where 28,30-bisnorhopane is also recorded, in particular in the latter well. In addition, the T4 seam exhibits the highest homohopane index of all seams in the West Lulu-1 and Lulu-1 wells. Seam T4 marks the last extensive peat accumulation in the Søgne Basin before the sea transgressed over the area. Above seam T4, lagoonal deposits overlain by transgressive shoreface and shelf deposits are preserved in Amalie-1, whereas transgressive shoreface and shelf deposits directly overlie seam T4 in Lulu-1 (Figs 7–9). The most landward part of seam T4 in the West Lulu-2 well is overlain by tidal channel and delta sediments followed by beach and outer shelf and offshore deposits.

Varying, but commonly high inertinite contents are a general feature of the Bryne Formation coals. Periods with comparatively slow watertable rises, possibly occasionally combined with doming of the peat surface, may have promoted watertable fluctuations, which may have favoured the formation of oxidation-derived inertinite as recently demonstrated in the Palangkaraya peat deposit, Kalimantan Tengah, Indonesia (Moore *et al.* 1996). However, the presence of char and pyrolytic carbon and the occurrence of pyroinertinite in all seams also imply a generally high frequency of wildfires in the mire systems. Thus, a seasonal climate with temporarily drier periods would enhance the possibility for drops in the watertable level below the peat surface and the ignition of fires. Reconstruction of precipitation suggests a seasonal wet climate for the region during the Early–Mid Jurassic (Parrish *et al.* 1982; Hallam 1985), and this is corroborated by annual rings in Lower–Middle Jurassic wood from Jameson Land in East Greenland and the island of Bornholm in the Baltic Sea (Fig. 1; Höhne 1933; Harris 1937; Nielsen 1995; Surlyk *et al.* 1995). Additionally, Cope (1993) observed an abundance of charcoalified material in cores from deltaic sediments of the Middle Jurassic Brent Group in the North Sea. Inertinite in mid-Cretaceous coals in the Gates Formation, Canada, was likewise interpreted to be exclusively fire-derived; formation occurred during periodic drought in the wetland settings (Lamberson *et al.* 1996). The somewhat uneven distribution of the inertinite in the Bryne Formation coals is probably to some degree related to the level of the watertable (wetness of the peat), but investigations of recent mire systems show that wildfires also may be related to the vegetation (Cohen & Stack 1996).

Influence of relative sea-level changes on coal composition

Siliciclastic deposits suggest a progressive southward transgression of the deeper eastern part of the Søgne Basin during the Bathonian–Callovian which during the Callovian gradually flooded the western part of the basin (Johannessen & Andsbjerg 1993; Andsbjerg 1997). Peat mires were established on the coastal plains west-south-west off the palaeo-shoreline. In particular the organic geochemistry of the coal seams support this interpretation. Increased proportions of C_{27} sterane and higher homohopane indices towards the palaeo-coastline is strong evidence for prolonged infiltration of saline water into the peat mires from a sea lying to the east. The coal seams in the West Lulu-3 well generally exhibit the strongest terrestrial signature by having the highest relative proportion of C_{29} sterane and the lowest homohopane indices of all samples. This area of the mire systems was thus least influenced by the marine environment to the east. Likewise the landward stepping nature and overall transgressive trend of the coal-bearing succession is reflected in the vertical succession of the coal seams which shows an increased saline influence in the organic geochemical composition from seam R1 to T4. These observations support the assumption that relative sea-level changes may exert an important control on peat accumulation in coastal mires. This is caused by the hydrological contact between sea water and groundwater in coastal settings, where the level of groundwater table and sea level more or less coincide (Diessel 1994). A relative sea-level rise will raise the watertable or base level on the coastal plain creating the necessary accommodation space for peat accumulation in a large, low-lying area with stagnant water and sedimentary bypass or ponding upstream, conditions very suitable for peat formation (e.g. Arditto 1991; Hartley 1993; Kosters & Suter 1993; Aitken 1994; Flint *et al.* 1995; Petersen & Andsbjerg 1996). The part of the precursor mires located closest to the palaeo-shoreline was most strongly influenced by base-level rise and the rate of peat accumulation was therefore more rapidly outpaced by the rate of watertable rise than in mire areas situated landward. This is reflected in the thinning of the coal seams in a seaward direction (Table 6). Thus, the rate of base-level rise and the position of the coal seams in the sequence stratigraphic framework may be reflected in their organic petrographic and geochemical composition (e.g. Diessel 1992; Banerjee *et al.* 1996; Petersen *et al.* 1996, 1998), which may have implications for the petroleum generative potential. For example, coal facies cycles formed by watertable rises or inundations linked to relative sea-level changes on Hochstetter Forland, North-East Greenland, are characterised by liptinite-enrichment towards the top of each cycle (Petersen *et al.* 1998). This has resulted in coal facies (dull lithotype) with extraordinarily high HI values (average: 464), and thin intercalated carbonaceous mudstones have an average HI of 459. Furthermore, Petersen *et al.* (1996) noticed a tendency to higher HI values and thermally extracted and generated hydrocarbon contents, S_1+S_2, in the T1–T4 seams compared to seams R1–R2 in the West Lulu-2 well. The highest avarage HI values in West Lulu-1 are likewise recorded in seams T2–T4, and the highest S_1+S_2 contents were obtained from seam T3. In the Lulu-1 seam T4 has the highest average HI value and seam T2 gives the highest S_1+S_2 contents.

Organic maturity

The majority of the vitrinite reflectance values obtained from the coal seams in West Lulu-3, West Lulu-1, Lulu-1 and West Lulu-2 (West Lulu-2 data from Petersen *et al.* 1996) range between 0.81 %R_m and 0.89 %R_m, while a minor proportion yields slightly lower values, 0.75–0.78 %R_m (Fig. 37). The latter values are measured in samples from coal seams T1, T3 and T4 and except for one outlier these coal samples are characterised by high vit-

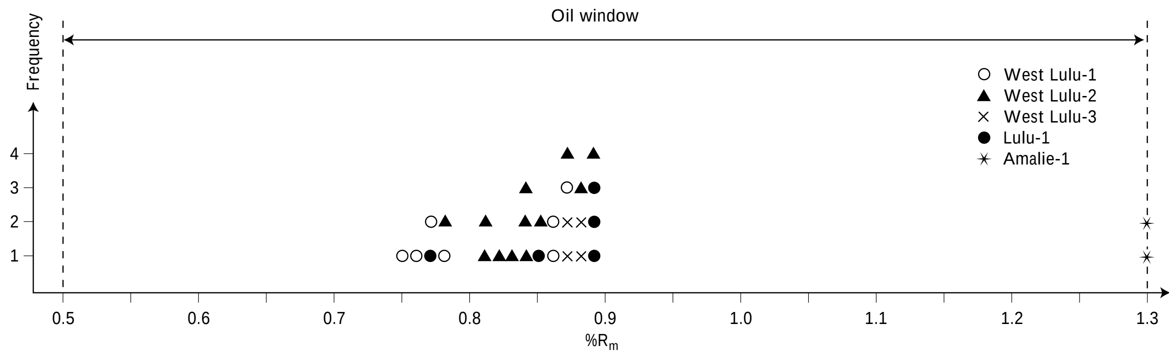

Fig. 37. Vitrinite reflectance values (%R_m) indicate that the coals in the West Lulu-1, -2, -3 and Lulu-1 wells with respect to thermal maturity are situated within the range of peak oil generation in the oil window (early catagenesis maturation stage). The much higher vitrinite reflectance values from the coals in the Amalie-1 well indicate that the organic matter with respect to thermal maturity is at the end of the oil window and is close to the late catagenesis maturation stage. West Lulu-2 data are from Petersen *et al.* (1996).

rinite contents (up to *c.* 84 vol.%) or high pyrite contents (up to *c.* 3 vol.%), or both. The retarded reflectance values are primarily related to hydrogen-enriched vitrinite, which has matured at a reduced rate (Petersen & Rosenberg 1998). The vitrinite precursor material was hydrogen-enriched during early diagenesis due to anoxic and occasionally marine-influenced conditions in the ancient mires. T_{max} values obtained from extracted coal samples, representing the total vitrinite reflectance range shown by the coals, do not indicate T_{max} suppression. However, T_{max} values obtained from hydrogen-enriched vitrinite concentrates show a slight T_{max} suppression compared to T_{max} values obtained from concentrates of 'normal' vitrinite (Petersen & Rosenberg 1998).

All reflectance values correspond to high volatile bituminous B/A rank and with respect to thermal maturity the coals are situated within the maturity range of peak oil generation in the 'oil window' (early catagenesis maturation stage) (Fig. 37). The oil window is situated between vitrinite reflectances of *c.* 0.5 %R_m and 1.3 %R_m with peak oil generation occurring between *c.* 0.8–1.0 %R_m (Hunt 1996). The average T_{max} values, ranging from 440°C to 444°C in the West Lulu-3, West Lulu-1 and Lulu-1 wells, are compatible with the reflectance values and confirm the coals to be in the early catagenesis stage of maturation (Hunt 1996, fig. 10-38, p. 389).

T_{max} values obtained from vitrinite lenses in Cleo-1 are comparable to the above results, while coaly mudstones yield higher pyrolysis temperatures. These latter samples are, however, also characterised by lower HI values possibly suggesting the presence of oxidised (inert) organic matter which may increase T_{max} (Peters 1986). The approximately 1000 m deeper burial depth of the organic matter in the Cleo-1 well compared to coals in the West Lulu-1, -2 and -3 wells and in Lulu-1 may on the other hand render a higher maturity. Excluding the two vitrinite lenses, the average T_{max} value is 456°C, i.e. approximately equivalent to a vitrinite reflectance of 1.1 %R_m (cf. Hunt 1996, fig. 10-38, p. 389), which may seem to be a reliable value compared to the Amalie-1 well (discussed below). A reflectance of 1.1 %R_m suggests a level of maturity in the late oil window.

The reflectance values of 1.3 %R_m obtained from seam T4 in Amalie-1 indicate that the organic matter with respect to thermal maturity is at the end of the oil window and is entering the late catagenesis maturation stage where mainly condensates and wet gas are formed. The coals are thus post-mature for oil generation. An average T_{max} value of 468°C is in very good agreement with the reflectance values. The high level of thermal maturity of the coals in the studied Amalie-1 succession is related to burial of *c.* 5000 m. The proposed reflectance value of 1.1 %R_m for the organic matter in Cleo-1 and the reflectance value of 1.3 %R_m in Amalie-1 would thus be in agreement with the *c.* 400 m deeper burial of the Amalie-1 well coals. According to the vitrinite reflectance values obtained from Amalie-1 and suggested for Cleo-1, a significant vitrinite reflectance increase is observed from *c.* 3500–5000 m burial depth. The higher rate of reflectance increase is a function of the exponential nature of vitrinite reflectance, in particular caused by the formation of polycyclic aromatic units above a reflectance value of 0.7 %R_o (Carr & Williamson 1990; Levine 1993).

The homohopane C_{31}–C_{35} epimer ratios between 0.57 and 0.67, with the majority of C_{29} sterane ratios between 0.45 and 0.50, and the majority of the αββ20(S+R)/[αββ20(S+R)+ααα20(S+R)] ratios between 0.50 and 0.64 indicate that the transformation ratios of these organic geochemical parameters have reached equilibrium (cf. Waples & Machihara 1991; Peters & Moldowan 1993) in the West Lulu-1, West Lulu-2, West Lulu-3, Lulu-1, Cleo-1 and Amalie-1 wells. The ratios are thus consistent with the level of maturity yielded by the vitrinite reflectance and T_{max} values. CPI values close to 1 indicate the absence of odd carbon-numbered *n*-alkane predominance in the heavy-end range, which is related to cleavage reactions at this level of maturity (Radke *et al.* 1980a).

Petroleum generative potential

The coals of the West Lulu-1 and -3 wells and the Lulu-1 well with respect to thermal maturity are in the phase of peak oil generation within the oil window. Despite the fact that the level of maturity indicates the coals have been depleted in hydrogen, they yield HI values above 200. Total average HI values for all coal samples within each of the wells West Lulu-1, West Lulu-3 and Lulu-1 are 180, 178 and 200, respectively, suggesting the coals are still capable of generating liquid and gaseous petroleum (Fig. 27). The coaly mudstones have HI values within the same range as the coals. This is related to the composition of the disseminated organic material, which is composed of macerals similar to the coals. Therefore, no evidence for a higher generative potential of the intercalated coaly mudstones can be demonstrated, a result in agreement with observations by Cook & Struckmeyer (1986).

Based on rank data, coals in the Amalie-1 well are post-mature with respect to liquid petroleum generation, but gas potential may still be present. The high rank of the coals results in generally low HI values and S_1+S_2 yields caused by exhaustion of the petroleum potential. However, HI values at *c.* 130 at the present level of maturity suggest that the coals may have generated liquid petroleum at a lower level of maturity.

With the exception of the vitrinite-lens samples and four sidewall core samples, HI values of samples from Cleo-1 are below 130 (Fig. 28; Table 12). This indicates a generally poor generative potential of the organic matter. Core samples represent floodplain and possibly tidally-influenced fluvial channel environments. Both environments may be well-drained, with the possibility for the disseminated organic debris to be redistributed and oxidised. This would account for gas-prone kerogen types III and IV with a small generative potential.

Seams T3 and T4 generally yield the highest average HI values and average thermal extracted and generated petroleum content, S_1+S_2, in West Lulu-3, West Lulu-1 and Lulu-1 (Table 11). Thus, generally the T-seams in individual wells show the higher HI values and S_1+S_2 yields and the R-seams the lower values. The extraordinary high value of HI=331 in West Lulu-3 contributes to the high average values of seam R1 in this well. In addition, for individual seams an increase in the average HI values is generally recorded in a seaward direction. These observations strongly suggest an influence of the depositional setting on the generative potential of the seams. The T-seams are interpreted to have formed during a comparatively fast rise in relative sea-level promoting a continuously high-standing watertable in the precursor mires and favouring prolonged influence of saline water, particularly in the low-lying reaches of the mires towards the palaeo-shoreline. Such conditions would, in general, create an anoxic peat mire with high activity of anaerobic bacteria, which favours the preservation of hydrogen-enriched vitrinitic precursor material and lipid substances (e.g. Khorasani 1987; Hunt 1996). Hydrogen-enriched (per-hydrous) vitrinite or vitrinite impregnated with absorbed bitumen may in particular be important progenitors of petroleum generation (Petersen & Rosenberg 1998), the formation of which is shown by development of secondary fluorescence. The general fluorescence of both collotelinite and collodetrinite thus suggests petroleum generative capability of the vitrinite, which may partly compensate for the low content of liptinite macerals in the coals (Fig. 25). Comparison of the seams in all wells reveals that the coal seams have the strongest terrestrial signature (highest Pr/Ph ratios, highest proportion of C_{29} steranes, lowest average homohopane index) in West Lulu-3. Thus, the landward position of West Lulu-3 and the general isolation from marine influence in this area during peat formation are not ideal conditions for the formation of hydrogen-enriched vitrinite, and this may explain why low or the lowest HI values and S_1+S_2 yields are recorded in this location.

These findings are corroborated by the multivariate regression analysis. The influence of the variables on S_2 is illustrated by the target coefficients, where the explained variances of the variables are projected on S_2 (Fig. 38). The target projection can be used to study the relation of each variable to S_2, that is a large bar in a negative direction indicates a variable with strong negative correlation to S_2, whereas a positive bar indicates a positive correlation to S_2. Intercorrelation between the variables is introduced by the closed data set, and the target projection can thus only be interpreted with an understanding of this limitation. The TOC content has a strong positive influence on the generative potential, as have vitrinite-rich components, in particular vitrite, clarite, duroclarite, collotelinite, telinite and the vitrinite maceral group (Fig. 38). Generally collodetrinite is considered to be more oil-prone than collotelinite due to its close association with liptinite and because of the lower reflecting, commonly fluorescent vitrinite particles hinting the presence of absorbed hydrocarbons. However, in this study and also in the earlier study by Petersen *et al.* (1996) the significance of collodetrinite alone on the remaining generative potential is nil, whereas the structured, frequently fluorescent telinite and in particular collotelinite macerals seem to be very important components. The absolute effect of telinite may, however, be limited due to the generally low content of this maceral. The combined effect of all the different vitrinite macerals on the generative potential is significant, and this is also stressed by the positive correlation between S_2 and the vitrinite-rich microlithotypes. These results emphasise the importance of the vitrinite components on the petroleum generative potential of coal-bearing strata.

Of the liptinite macerals only resinite shows an important influence on the remaining generative potential (Fig. 38). Sporinite exhibits a weak positive correlation, but surprisingly cutinite shows a strong negative correlation to the remaining S_2. The absolute effect of cutinite is small as 48% of the samples only contain from 0 to 0.3 vol.% of cutinite. Due to the wide range of acti-

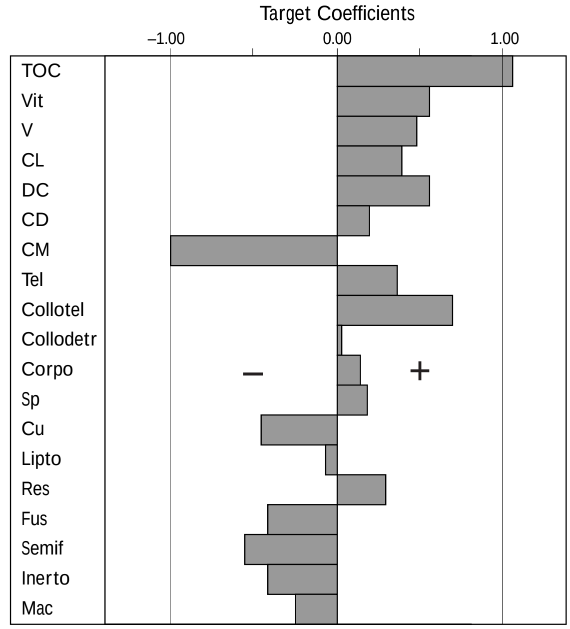

Fig. 38. Target projection of the partial least squares regression (PLSR) model, which gives a measure of the correlation between individual variables and S_2. The TOC content, vitrinite, vitrite, clarite, duroclarite, collotelinite and telinite are in particular positively correlated to the remaining generative potential S_2. TOC = total organic carbon; Vit = vitrinite maceral group; V = vitrite; CL = clarite; DC = duroclarite; CD = clarodurite; CM = carbominerite; Tel = telinite; Collotel = collotelinite; Collodetr = collodetrinite; Corpo = corpogelinite; Sp = sporinite; Cu = cutinite; Lipto = liptodetrinite; Res = resinite; Fus = fusinite; Semif = semifusinite; Inerto = inertodetrinite; Mac = macrinite.

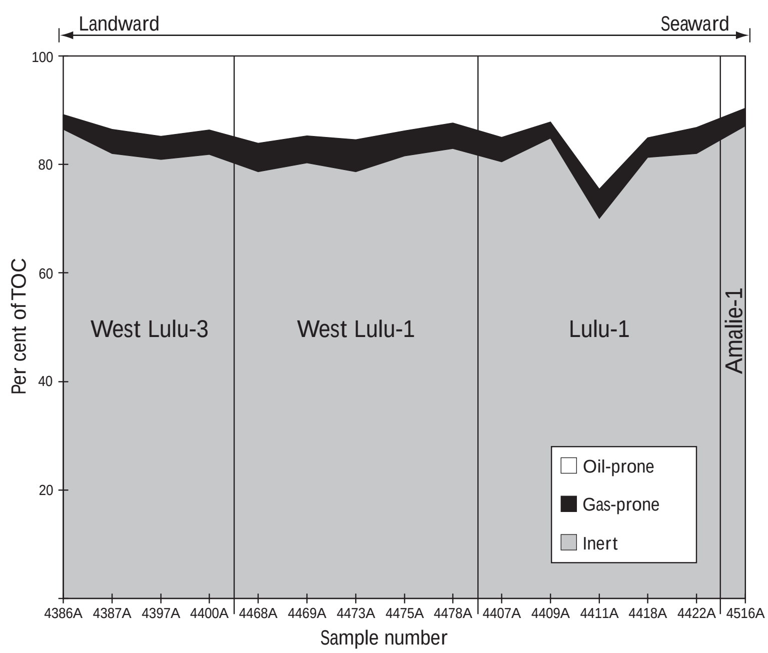

Fig. 39. The proportion of oil-prone, gas-prone and chemically inert carbon in the coals from West Lulu-3, West Lulu-1 and Lulu-1 wells computed by combining Rock-Eval and Py-GC data. The majority of the carbon in the coals is chemically inert with respect to petroleum generation. However, the graph shows that between 13% and 30% of the carbon will contribute to the formation of petroleum during maturation. Note the high proportion of oil-range components (C_{6+}) which constitute between 72.4% and 82.0% of the total pyrolysate, whereas gas-range components ($C_{1–5}$) only constitute between 18.0% and 27.6% of the pyrolysate.

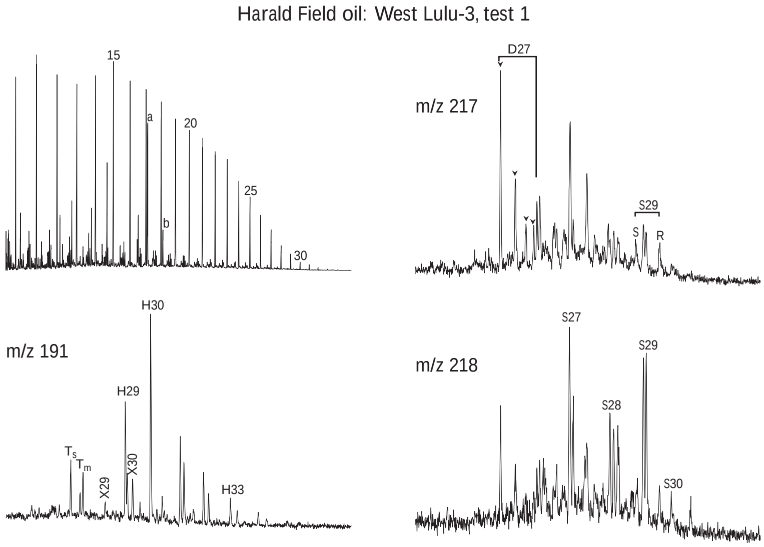

Fig. 40. An example of an oil/condensate derived from the Bryne Formation in the West Lulu-3 well. A typical terrestrial composition is shown by a Pr/Ph ratio of 4.24, a hopane distribution which maximises at C_{30}, and a $C_{27–29}$ sterane distribution dominated by the C_{29} sterane (44%). The compositional similarity to the coal extracts shown in Fig. 30 is evident. Annotation: numbers on GC-trace refer to *n*-alkane carbon numbers, a: pristane, b: phytane; T_s: trisnorneohopane, T_m: trisnorhopane, H29: norhopane, H30: hopane, H33, trishomohopane, X29: dianorhopane, X30: diahopane; D27: C_{27} diasteranes (4 isomers), S27, S28, S29 and S30: $C_{27–30}\alpha\beta\beta$ regular steranes, S: $C_{29}\alpha\alpha\alpha$(20S), R: $C_{29}\alpha\alpha\alpha$(20R).

vation energies of the different macerals in coals they do not release petroleum simultaneously, but generation of individual components is dependent on the thermal history of the coal (Boreham & Powell 1993). It may tentatively be suggested that the generative capacity of cutinite at the present level of maturity is limited, resulting in a negative correlation to S_2.

As expected the carbon-rich and hydrogen-poor inertinite macerals exhibit a negative correlation to S_2 (Fig. 38). Likewise the mineral-rich microlithotype carbominerite has a negative impact on the generative potential.

Using the classification scheme of Larter (1985), which is based on Py-GC, the pyrolysates from the 15 solvent-extracted Bryne Formation coals closely resemble the "II/IIIpp type" kerogen. This kerogen type is recognised by the presence of abundant aliphatic as well as aromatic/phenolic moieties in the pyrolysate, and is held to be present mainly in marine deposits containing high proportions of predominantly vitrinitic and liptinitic terrestrial organic debris. The abundance of aliphatic moieties is generally accounted for by the presence of highly aliphatic liptinite macerals such as cutinite and alginite, whereas the aromatic phenolic moieties are assumed to originate from vitrinite and sporinite. However, in the present case, none of the coal samples contain notable proportions of liptinite macerals, and the abundance of aliphatic moieties may thus also point to the presence of hydrogen-enriched (perhydrous) vitrinite or submicroscopical liptinite.

The oil-prone nature of the Bryne Formation coals discussed in previous paragraphs is strongly supported by evidence from Py-GC. An estimate of the fractions of TOC of oil-prone, gas-prone and chemically inert carbon may be computed by combining Rock-Eval and Py-GC data (Pepper & Corvi 1995). This calculation shows that although most carbon contained in the coals is chemically inert in the sense that it will not contribute to the petroleum product potentially generated during thermal maturation, between 13 and 30% of the carbon may, at the present level of maturity, potentially participate in the formation of petroleum products, i.e. oil and gas (Fig. 39). All pyrograms show the presence of very high proportions of oil-range components (C_{6+}), which constitute from 72.4% to 82.0% of the total pyrolysate (Figs 32, 39). Gas-range components ($C_{1–5}$) are but minor constituents, which constitute from 18.0% to 27.6% of the pyrolysate.

There is a tendency towards increased proportions of oil-like components in pyrolysates from the more marine-influenced Lulu-1 well coals. Furthermore, the fractions found for the partitioning of 'gas' and 'oil' components correspond well to the results of Pepper & Corvi (1995), which show 'gas' fractions of 0.2 to 0.3 for samples with HI values similar to those of the samples analysed in this study. With respect to petroleum generation, the maturity of the samples is comparatively high. However the data indicate that considerable generation of petroleum remains to take place before the full potential is eventually realised. This observation corroborates the idea of progressive generation over a wide span of thermal maturities from rocks dominated by terrestrial kerogen (e.g. Bordenave *et al.* 1993).

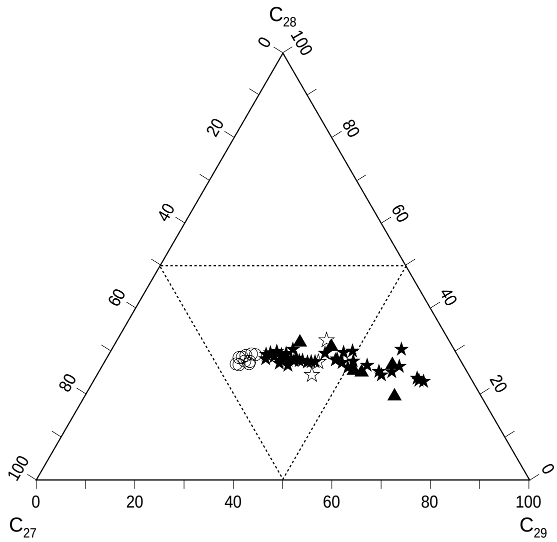

Fig. 41. Normalised $C_{27–29}$ sterane distribution in 58 Bryne Formation coal extracts (including West Lulu-2 data from Petersen *et al.* 1996), 8 Bryne Formation coaly mudstone extracts, 3 Harald Field derived oils/condensates and 19 Farsund Formation derived oils (data from Bojesen-Koefoed *et al.* 1994). Extracts from both the coals and the intercalated mudstones are dominated by C_{29} sterane, and show a sterane distribution very similar to the sterane distribution of the Harald Field oils/condensates. The sterane distribution of the Farsund Formation derived oils differ by having a higher proportion of C_{27} sterane.

The discussion on the ability of coals to expel liquid petroleum was discussed earlier, and implications for the expulsion capability of the West Lulu-2 coals was discussed in Petersen *et al.* (1996). Two commercial gas and oil accumulations in the Harald Field (expected reserves, oil: 7 million m^3, gas: 25 billion Nm^3; Danish Energy Agency 1997) and the Lulita discovery (which contains a high-wax terrigenous oil; GEUS, unpublished data) are indirect evidence for the capability of the coals to expel petroleum. As described above no petrographic or geochemical data point to a better generative potential of the intervening carbonaceous mudstones rendering the coals the likely source rock. Three oil/condensate samples recovered from Bryne Formation sandstones in West Lulu-1 and West Lulu-3 display similar maturity as the coals and they have a typical terrestrial composition (Fig. 40), including Pr/Ph ratios between 4.09 and 4.24, a hopane distribution which maximises at C_{30}, and bulk isotope $\delta^{13}C$ ratios of up to or greater than –26‰, which is significantly heavier than the common oils generated from the marine Farsund Formation (Petersen *et al.* 1995, 1996). The Harald Field oil/condensate samples also differ from Farsund Formation derived oils by having a higher proportion of C_{29} sterane. However, the sterane distribution of the oil/condensate samples is very similar to the sterane distribution of the Bryne Formation coal extracts (Figs 30, 40, 41). Sterane distribution of intercalated coaly mudstone extracts is likewise dominated by C_{29} sterane. In Amalie-1, a condensate recovered from the Bryne Formation likely consists of a mixture of material generated from terrestrial and marine source rocks (Statoil, unpublished data; GEUS, unpublished data). The condensate has a bulk isotope $\delta^{13}C$ ratio of –25.26‰ and, based on gas from the same test, a maturation level corresponding to a vitrinite reflectance of 1.3 %R was assumed, a maturity which corresponds exactly to the vitrinite reflectance values obtained from the coals (Fig. 37). Thus, this evidence supports the contention that petroleum has been released from the coals. Hunt (1996) describes a 'migration index' (MI) defined as S_1/TOC and suggests MI values between 0.1 and 0.2 for oil expulsion. According to this index all coal seams and carbonaceous mudstones are able to expel liquid petroleum (Table 15). The West Lulu-2 coals show MI values from 0.23 to 0.27, whereas the MI values of the coals in the West Lulu-3, West Lulu-1 and Lulu-1 wells range from 0.15 to 0.21. The West Lulu-3 well exhibits the lowest values, which is in agreement with generally lower HI values and S_1+S_2 yields of the seams in this well (Table 11). Seams R1 and T4 in Amalie-1 show lower MI values which are related to the high thermal maturity. MI values of the mudstones are lower or similar to the MI values of the coals, which again reject the intercalated carbonaceous mudstones as a more significant source rock than the coals.

Table 15. Average of Migration Index, S_1/TOC

Well / Seam	W. Lulu-2	W. Lulu-3	W. Lulu-1	Lulu-1	Amalie-1
T4	0.25	-	0.19	0.21	0.13
T3	0.25	-	0.21	-	-
R2	0.25	-	-	-	-
T2	0.24	0.19	0.19	0.20	-
R1a	-	0.15	0.19	-	-
R1	0.23	0.16	0.18	0.19	0.13
T1	0.27	-	-	-	-
Mudstones	0.17	0.16	0.19	0.23	0.16